This is an open access article published under a Creative Commons Non-Commercial No Derivative Works (CC-BY-NC-ND) Attribution License, which permits copying and redistribution of the article, and creation of adaptations, all for non-commercial purposes.

ACS AUTHORCHOICE

molecular pharmaceutics

pubs.acs.org/molecularpharmaceutics

Article

EGFR-Targeted Nanobody Functionalized Polymeric Micelles Loaded with mTHPC for Selective Photodynamic Therapy

Yanna Liu, Luca Scrivano, Julia Denise Peterson, Marcel H. A. M. Fens, Irati Beltrán Hernández, Bárbara Mesquita, Javier Sastre Toraño, Wim E. Hennink, Cornelus F. van Nostrum, and Sabrina Oliveira*

Cite This: *Mol. Pharmaceutics* 2020, 17, 1276–1292

Read Online

ACCESS | Metrics & More | Article Recommendations | Supporting Information

ABSTRACT: *meta*-Tetra(hydroxyphenyl)chlorin (mTHPC) is one of the most potent second-generation photosensitizers, clinically used for photodynamic therapy (PDT) of head and neck squamous cell carcinomas. However, improvements are still required concerning its present formulation (i.e., Foscan, a solution of mTHPC in ethanol/propylene glycol (40:60 w/w)), as mTHPC has the tendency to aggregate in aqueous media, e.g., biological fluids, and it has limited tumor specificity. In the present study, polymeric micelles with three different diameters (17, 24, and 45 nm) based on benzyl-poly(ε-caprolactone)-*b*-poly(ethylene glycol) (PCL_n-PEG; n = 9, 15, or 23) were prepared with mTHPC loadings ranging from 0.5 to 10 wt % using a film-hydration method as advanced nanoformulations for this photosensitizer. To favor the uptake of the micelles by cancer cells that overexpress the epidermal growth factor receptor (EGFR), the micelles were decorated with an EGFR-targeted nanobody (named EGa1) through maleimide-thiol chemistry. The enhanced binding of the EGFR-targeted micelles at 4 °C to EGFR-overexpressing A431 cells, compared to low-EGFR-expressing HeLa cells, confirmed the specificity of the micelles. In addition, an enhanced uptake of mTHPC-loaded micelles by A431 cells was observed when these were decorated with the EGa1 nanobody, compared to nontargeted micelles. Both binding and uptake of targeted micelles were blocked by an excess of free EGa1 nanobody, demonstrating that these processes occur through EGFR. In line with this, mTHPC loaded in EGa1-conjugated PCL_{23}-PEG (EGa1-P_{23}) micelles demonstrated 4 times higher photocytotoxicity on A431 cells, compared to micelles lacking the nanobody. Importantly, EGa1-P_{23} micelles also showed selective PDT against A431 cells compared to the low-EGFR-expressing HeLa cells. Finally, an *in vivo* pharmacokinetic study shows that after intravenous injection, mTHPC incorporated in the P_{23} micelles displayed prolonged blood circulation kinetics, compared to free mTHPC, independently of the presence of EGa1. Thus, these results make these micelles a promising nanomedicine formulation for selective therapy.

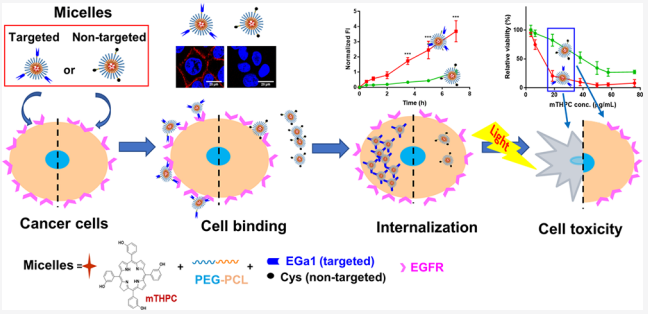

KEYWORDS: *nanobody, targeting, polymeric micelles, selectivity, photodynamic therapy, EGFR*

1. INTRODUCTION

Head and neck squamous cell carcinomas (HNSCC) are the sixth most prevalent malignancy globally, involving carcinomas in the mouth, throat, larynx, sinuses, and lymph nodes of the neck and responsible for more than 650 000 new cases and about 330 000 deaths annually.[1,2] Photodynamic therapy (PDT) has attracted much attention in recent years as a treatment modality for HNSCC. This topical and minimally invasive treatment has decreased the likelihood of adverse side effects, such as late organ dysfunction, xerostomia, and dysphagia, which are associated with conventional modalities, such as surgery and radiotherapy.[3−5] PDT involves illumination of oxygenated tissue after the systemic administration of a photosensitizer (PS).[6−8] The PS is activated by light of the absorbed wavelength, locally applied in the abnormal tissue by surface illumination or optical fibers.[6] The activated PS subsequently transfers its energy to nearby molecular oxygen, producing oxygen radicals and other reactive oxygen species (ROS). These ROS in turn cause oxidation of cellular components such as nucleic acids, proteins, and lipids, inducing cellular apoptosis and/or necrosis, which subsequently leads to breakdown of tumor associated vasculature and immune stimulation for tumor destruction.[6,9]

Received: December 18, 2019
Revised: March 6, 2020
Accepted: March 6, 2020
Published: March 6, 2020

© 2020 American Chemical Society

https://dx.doi.org/10.1021/acs.molpharmaceut.9b01280
Mol. Pharmaceutics 2020, 17, 1276–1292

The highly potent, second-generation PS, *meta*-Tetra(hydroxyphenyl)chlorin (mTHPC), also known by its generic name temoporfin, has many advantages over first-generation photosensitizers (e.g., stronger phototoxicity and a longer absorption wavelength, which is beneficial for light penetration in tumor tissue).[10,11] Its commercial formulation, Foscan (solution in ethanol/propylene glycol 40:60 w/w), has been approved for PDT of HNSCC.[1,10] However, like most of the photosensitizers, mTHPC's hydrophobic characteristic (logP ≈ 9) promotes nonspecific binding to cells, resulting in a disposition of PS also in normal healthy tissues (i.e., no selective accumulation of the PS in tumorous tissues), which is responsible for damage to surrounding health tissues and the frequently observed and unwanted cutaneous photosensitivity in patients.[9,11−13] Additionally, upon administration, mTHPC is prone to aggregation in biological fluids, leading to lower ROS production and decreased therapeutic efficacy.[14,15]

To address these drawbacks, two liposomal mTHPC formulations are currently on the market: Foslip and its PEGylated form FosPEG, in which a polyethylene glycol (PEG) coating on the surfaces of the liposomes provides stealth characteristics, preventing its recognition and rapid uptake by the reticuloendothelial system (RES) and resulting in longer circulation in blood.[13,16−18] Both liposomal mTHPCs have the ability to package large quantities of mTHPC into their lipid bilayers, and several publications describe some improvements regarding the selective accumulation of mTHPC in tumors due to the enhanced permeability and retention (EPR) effect,[19−21] even though both formulations showed a rapid release of the payload in the first 3 h after injection.[13,18,22] However, the relatively large hydrodynamic diameters of those liposomes (∼110 nm) can cause heterogeneous distribution in the tumor tissues and inability to penetrate the tumor interstitial matrix to reach the interior tumor cells, which can compromise their therapeutic efficacy.[23−27]

Polymeric micelles, consisting of a hydrophilic stealth corona (most commonly based on PEG) and a hydrophobic core that is suitable for accommodating hydrophobic compounds, are attractive and alternative drug delivery systems for hydrophobic drugs, particularly cytostatic agents.[28−31] Most importantly, polymeric micelles have small hydrodynamic diameters that can be tailored by the composition and molecular weight of the micelles forming block copolymers as well as by the processing conditions.[32−34] Their small size, generally below 60 nm, makes them more suitable to extravasate the bloodstream, be retained at the tumor through the EPR effect (passive targeting), and subsequently penetrate into the interior of the tumor with uniform distribution, all crucial factors for antitumoral efficacy of nanomedicines.[23,25,35]

After passive accumulation in tumors, furnishing a specific ligand on the surfaces of micelles was proposed to compensate for the potentially diminished uptake by the target cells due to the hydrophilic PEG layer and also to favor the intracellular internalization of the active payload by the target cancer cells.[36−39] Many cancer cells overexpress receptors that can be recognized by and interact with specific ligands, such as growth factors, antibodies, antibody fragments, or peptides, leading to enhanced target cell internalization of nanoparticles that have their surface decorated with these ligands.[40] A well-explored receptor in the context of HNSCC is the epidermal growth factor receptor (EGFR).[41] Nanobodies are small antibody fragments originated from heavy-chain-only antibodies present in the blood of Camelidae. Also known as single domain antibodies, they are characterized by their small size, high stability, low immunogenic potential, and high binding affinities to their antigens.[42−44] The EGFR-targeted nanobody EGa1 has demonstrated its ability to bind to EGFR and be internalized by EGFR-overexpressing cells, when conjugated to the surfaces of liposomes and polymeric micelles, without triggering EGFR's cascade of events for growth promotion.[38,43] It is worth noting that studies have suggested that small micelles especially in the hydrodynamic diameter range of 60 nm or less would be favorable for effectively binding the receptor and inducing receptor-mediated endocytic processes.[26,45−48]

In the present study, we synthesized poly(ε-caprolactone)-*b*-methoxypoly(ethylene glycol) (PCL_n-PEG) based copolymers with varying chain lengths of PCL_n (n = 9, 15, 23) and a fixed molecular weight of PEG (2 kDa) and used film hydration of these polymers to prepare mTHPC-loaded micelles with diameters less than 50 nm. Previously, we showed that PCL-PEG micelles (around 28 nm in size) decorated with an EGFR-targeted nanobody were selectively taken up by high-EGFR-overexpressing A431 cells, compared to EGFR-negative E98 cells.[49] To further eleborate on this observation, in the present work, we decorated the micelles having three different diameters (17, 24, and 45 nm) with the EGFR-targeted nanobody EGa1, using maleimide-thiol click chemistry.[50] The cellular binding and uptake of these micelles loaded with mTHPC were evaluated by confocal fluorescence microscopy, using the EGFR-overexpressing A431 cell line and the low-EGFR-expressing HeLa cell line. The photocytotoxicity of the micellar PS formulations was evaluated on both cell lines to reveal the potential of these formulations to improve the selectivity of PDT to EGFR-overexpressing tumor cells. Finally, the *in vitro* stability and the *in vivo* pharmacokinetics of these micellar mTHPC formulations were studied in human plasma and A431 tumor-bearing mice, respectively.

2. EXPERIMENTAL SECTION

2.1. Materials. Poly(ethylene glycol) methyl ether amine (PEG-NH_2, 2000 g/mol) was synthesized as previously reported.[51] *N*-Succinimidyl-*S*-acetylthioacetate (SATA, Pierce) was purchased from Thermo Fisher Scientific (Massachusetts, USA). Maleimide-poly(ethylene glycol)-amine trifluoroacetic acid (Mal-PEG-NH_2·TFA, 2000 g/mol) was purchased from JenKem Technology (Dallas, USA). *m*-Tetra(hydroxyphenyl)-chlorin (mTHPC) was obtained from Molekula (Munich, Germany). Optimem phenol red free (OptiMEM) was purchased from Invitrogen (Bleiswijk, The Netherlands). Hoechst 33342 solution (20 mM) was purchased from Thermo Fisher (Bleiswijk, The Netherlands). CellTiter 96 AQueous One Solution was obtained from Promega (Leiden, The Netherlands). All other reagents and deuterated chloroform ($CDCl_3$), dichloromethane (DCM), and toluene were obtained from Sigma-Aldrich (Zwijndrecht, The Netherlands). Phosphate-buffered saline (PBS, pH 7.4, containing 11.9 mM phosphates, 137 mM sodium chloride, and 2.7 mM potassium chloride) was obtained from Fisher Bioreagents (Bleiswijk, The Netherlands). 7,9-Dioxa-2,3-dithiaspiro[4.5]decan-8-one (i.e., 1,2-dithiolane-substituted trimethylene carbonate, DTC) was kindly provided by Prof. Zhiyuan Zhong (Soochow University, SuZhou, China). Cyanine7 maleimide (Cy7-maleimide) was ordered from Lumiprobe Corporation (Hann-

https://dx.doi.org/10.1021/acs.molpharmaceut.9b01280
Mol. Pharmaceutics 2020, 17, 1276−1292

over, Germany). All other solvents were obtained from Biosolve (Valkenswaard, The Netherlands). DCM, ε-caprolactone (ε-CL), and toluene were dried over 4 Å molecular sieves (Sigma-Aldrich, Zwijndrecht, The Netherlands) prior to use. PEG-NH_2 and Mal-PEG-NH_2·TFA were dried overnight under vacuum at room temperature prior to use. All other reagents were used as received.

2.2. Synthesis of Copolymers. *2.2.1. Synthesis of Benzyl-poly(ε-caprolactone).* Benzyl-poly(ε-caprolactone)$_n$ (PCL_n-OH) with different degrees of polymerization were synthesized as previously described with a slight modification.[51] Benzyl alcohol (1.03 mL, 10 mmol) and ε-CL (6.09 mL (55 mmol), 15.74 mL (142 mmol), or 25.49 mL (230 mmol)) were introduced into a round flask and stirred at 130 °C under vacuum for 5 h to remove traces of water. Subsequently, $Sn(Oct)_2$ (0.02 mL, 0.5 mmol) was added, and the reaction was allowed to occur under a nitrogen atmosphere for 4 to 6 h (until the complete conversion of ε-CL, as monitored by ^{1}H NMR). After cooling down to room temperature (RT), the formed PCL oligomers were dissolved in 10 mL of DCM and purified by precipitation in a 20-fold excess of cold diethyl ether (−20 °C). The precipitated products were recovered by filtration, and the final products were obtained as a whitish powder after drying under vacuum overnight. ^{1}H NMR ($CDCl_3$): δ = 7.35 (b, aromatic protons, benzyl alcohol), 5.11 (s, CCH_2O), 4.05 (m, CH_2CH_2O), 3.65 (t, CH_2CH_2OH), 2.30 (m, $OC(O)CH_2$), 1.65 (m, $CH_2CH_2CH_2CH_2CH_2$), 1.38 (m, $CH_2CH_2CH_2CH_2CH_2$).

2.2.2. Synthesis of Benzyl-poly(ε-caprolactone)-p-nitrophenyl Formate. The terminal hydroxide group of PCL_n-OH was activated by nitrophenyl chloroformate (PNC) to obtain benzyl-poly(ε-caprolactone)-*p*-nitrophenyl formate (PCL_n-PNF) according to a previous procedure with slight modification.[51] In short, the above obtained PCL_n oligomers (4 g, corresponding to 3.5 mmol (n = 9), 2.2 mmol (n = 15), 1.5 mmol (n = 23)) were separately dissolved in 20 mL of dried toluene, followed by the addition of triethylamine (TEA) (1.8 mL (13 mmol) for n = 9, 1.1 mL (7.7 mmol) for n = 15, or 0.7 mL (5.1 mmol) for n = 23) and PNC (2.64 g (13 mmol) for n = 9, 1.6 g (7.7 mmol) for n = 15, 0.5 g (5.1 mmol) for n = 23) with agitation. The reaction proceeded overnight with magnetic stirring at RT under a nitrogen atmosphere. The formed TEA·HCl precipitate was removed by centrifugation (5000 rpm, RT). The remaining supernatant was dropped into cold diethyl ether (−20 °C), and the precipitated solids were collected after filtration and drying under vacuum overnight. This procedure was repeated one time more, and the final products were obtained as white powders. ^{1}H NMR ($CDCl_3$): δ = 8.27 (d, aromatic protons, PNF), 7.38 (m, aromatic protons, benzyl alcohol and PNF), 5.11 (s, CCH_2O), 4.29 (m, $CH_2C\,H_2OC(O)O$), 4.05 (m, CH_2CH_2O), 2.30 (m, $OC(O)CH_2$), 1.65 (m, $CH_2CH_2CH_2CH_2CH_2$), 1.38 (m, $CH_2CH_2CH_2CH_2CH_2$).

2.2.3. Synthesis of Benzyl-poly(ε-caprolactone)-b-methoxy-poly(ethylene glycol). Benzyl-poly(ε-caprolactone)$_n$-*b*-methoxy-poly(ethylene glycol) (PCL_n-PEG) copolymers were synthesized as follows.[51] In brief, to a solution of PEG-NH_2 (0.6 g, 0.3 mmol) in 10 mL of dry toluene, the above obtained PCL_n-PNFs (0.3 mmol) were separately added. The reaction mixtures were stirred overnight at RT under a nitrogen atmosphere. Next, the obtained solutions (yellowish due to released *p*-nitrophenol) were dropped in diethyl ether at RT, and the yellowish polymer precipitates were collected after filtration. After the remaining organic solvent was evaporated under a nitrogen stream, the collected products were then suspended in deionized water and dialyzed (tubing with MWCO of 10 kDa) against water for 12 h to remove traces of the *p*-nitrophenol and unreacted PEG-NH_2. After freeze-drying, the final products were obtained as white powders. ^{1}H NMR ($CDCl_3$): δ = 7.35 (b, aromatic protons, benzyl alcohol), 5.11 (s, CCH_2O), 4.05 (m, CH_2CH_2O), 3.64 (m, PEG protons), 3.38 (s, OCH_3), 2.30 (m, $OC(O)CH_2$), 1.65 (m, $CH_2CH_2CH_2CH_2CH_2$), 1.38 (m, $CH_2CH_2CH_2CH_2CH_2$).

2.2.4. Synthesis of Benzyl-poly(ε-caprolactone)-b-poly(ethylene glycol)-maleimide. Benzyl-poly(ε-caprolactone)$_n$-*b*-poly(ethylene glycol)-maleimide (PCL_n-PEG-Mal) copolymers were synthesized as follows. Mal-PEG-NH_2·TFA (0.4 mg, 0.2 mmol) and dry TEA (0.3 mg, 0.24 mmol) were dissolved in 7 mL of dry toluene, and the above obtained PCL_n-PNFs (0.2 mmol) were added under stirring. The molar ratio of Mal-PEG-NH_2·TFA/TEA/PCL_n-PNF was 1:1.2:1. The reaction proceeded overnight at RT under a nitrogen atmosphere. The formed TFA·TEA salts were removed by centrifugation, and the remaining supernatants were dropped into diethyl ether at RT to precipitate the polymers, which was repeated twice. The products were obtained as light-brown solids after filtration and drying under vacuum. ^{1}H NMR ($CDCl_3$): δ = 7.35 (m, aromatic protons, benzyl alcohol), 6.70 (s, maleimide protons), 5.11 (s, CCH_2O), 4.05 (m, CH_2CH_2O), 3.64 (m, PEG protons), 2.30 (m, $OC(O)CH_2$), 1.65 (m, $CH_2CH_2CH_2CH_2CH_2$), 1.38 (m, $CH_2CH_2CH_2CH_2CH_2$).

Quantification of the maleimide functional group of PCL_n-PEG-Mal was done by ^{1}H NMR analysis, by calculating the integral ratio between peaks from maleimide protons at 6.70 ppm and CH_2 from the terminal benzyl group at 5.11 ppm. UV spectra of PCL_n-PEG-Mal copolymers in DCM (5 mg/mL) were recorded in the range of 240−350 nm using a quartz cuvette (1 cm) using a UV-2450 Shimadzu spectrophotometer, and the number of the maleimide groups per copolymer chain was also quantified by the absorption at 293 nm (maximum absorbance of maleimide group) and calibration by a series of Mal-PEG-NH_2 solutions in DCM.

2.2.5. Synthesis and Characterizations of Cy7 Labeled DTC-Containing Copolymer Based on Benzyl-poly(ε-caprolactone)-b-poly(ethylene glycol). Cy7 labeled polymer was synthesized in two steps. First, PCL-PDTC-PEG was synthesized using methanesulfonic acid (MSA) as the catalyst as previously described with slight modifications.[52,53] In short, CL (434 mg, 3.80 mmol), DTC (330 mg, 1.72 mmol), and mPEG-OH (421 mg, 0.21 mmol) were dissolved in 6 mL of dry DCM, followed by the addition of MSA (25 mg, 0.26 mmol) with agitation to initiate polymerization. The polymerization was conducted at 37 °C for 10 h under N_2 atmosphere, and then, TEA (equimolar to MSA) was added to terminate the reaction. The reaction solution was dropped into a 20-fold excess of cold diethyl ether (−20 °C), and the precipitate collected by filtration was dried under vacuum to give the final product as slightly yellow solid (809 mg, yield: 68%). ^{1}H NMR (600 MHz, $CDCl_3$): δ 4.29−4.00 (m, $COOCH_2CCH_2OCO$, CH_2OH), 3.63 (m, PEG protons), 3.37 (s, CH_3O), 2.97 (m, CCH_2SSCH_2C), 2.32 (m, $CH_2CH_2CH_2COO$), 1.65 (m, $CH_2CH_2CH_2CH_2CH_2$), 1.39 (m, $CH_2CH_2CH_2CH_2CH_2$).

In the second step, 1.5 mL of a solution of the mixture of PCL/PDTC-PEG copolymer and Cy7-maleimide in DMF (46.8 mg/mL of PCL/PDTC-PEG and 3.7 mg/mL of Cy7-maleimide) was added dropwise to 16.5 mL of water. The

https://dx.doi.org/10.1021/acs.molpharmaceut.9b01280
Mol. Pharmaceutics 2020, 17, 1276−1292

homogeneous dispersion was formed after gentle shaking by hands. A 550 μL aliquot of tris(2-carboxyethyl)phosphine hydrochloride (TCEP, 40 mg/mL in water) was added to the dispersion. The dispersion was stirred for 4 h at RT, followed by the addition of 100 μL of maleimide solution in DMF (150 mg/mL) to cap the unreacted free thiols and subsequent agitation for another 4 h. Finally, the dispersion was dialyzed with dialysis tubing (MWCO = 1 kDa) against THF/water (1:1, v/v), refreshing the dialysate after 24 h for in total three times, to remove the uncoupled Cy7-maleimide and maleimide. The final product was collected as a lightly green solid after lyophilization. To confirm the conjugation of Cy7 to the polymer, the resulting polymer was analyzed by GPC coupled with a UV−vis detector (detection wavelength of 700 nm) as described in Section 2.3. The amount of Cy7 coupled to the polymer was analyzed by recording the absorbance of Cy7 coupled polymer at 755.5 nm using a UV-2450 Shimadzu spectrophotometer and calculated using the calibration curve of a series of standard solutions of Cy7-maleimde in DMF with concentrations ranging from 0 to 2.5 μg/mL.

2.3. Polymer Characterization. ^{1}H nuclear magnetic resonance (^{1}H NMR) spectra were recorded using a Bruker NMR spectrometer (600 MHz, Bruker), with chemical shifts reported in parts per million downfield from tetramethylsilane. Polymers were dissolved in $CDCl_3$ at a concentration of around 10 mg/mL. The central line of residual solvents ($CHCl_3$: δ 7.26 ppm) was used as the reference line. Peak multiplicity was designated as s (singlet), d (doublet), dd (double doublet), t (triplet), q (quartet), m (multiplet), and b (broad signal).

Calculation of DP and M_n: The average degree of polymerization (DP) of the synthesized caprolactone oligomers was determined from the ratio of the integral of the CH_2 protons of the ε-CL units (4.05 ppm, CH_2CH_2O) to the CH_2 protons of the benzyl alcohol (5.10 ppm, CCH_2O). The number of ethylene oxide units in the polymers was calculated by the integral ratio of the CH_2 protons of the benzyl alcohol (5.10 ppm, CCH_2O) to CH_2 protons of the PEG units (3.64 ppm, PEG proton). The DP of CL and DTC in the obtained PCL-PDTC-PEG copolymer was determined from the ratio of the integral of the CH_2 protons of the CL units (1.39 ppm, $CH_2CH_2CH_2CH_2CH_2$), the protons of the DTC units (2.97 ppm, CCH_2SSCH_2C). The number-average molecular weight (M_n) of the copolymers was determined by ^{1}H NMR and calculated from the resulting number of caprolactone units and ethylene oxide units. The number-average molecular weight M_n, weight-average molecular weight M_w, and polydispersity (M_w/M_n) of the synthesized polymers were determined by gel permeation chromatography (GPC, Waters Alliance 2695 System), equipped with two PLgel Mesopore columns (300 × 7.5 mm, including a guard column, 50 × 7.5 mm). Dimethylformamide (DMF) containing 10 mM LiCl was used as the eluent at a flow rate of 1.0 mL/min at 65 °C. A differential refractive-index (RI) detector was used to record the chromatograms. Aliquots of 50 μL of 3−5 mg/mL polymer samples dissolved in DMF containing 10 mM LiCl were injected onto the column. Calibration was done using narrow poly(ethylene glycol) standards ranging from 430 to 26 100 g/mol, and the molecular weights of the PCL-PEG block copolymers were calculated using Empower 32 software.

2.4. Preparation and Characterization of Empty and mTHPC-Loaded Polymeric Micelles. Empty micelles based on PCL_n-PEG (n = 9, 15, or 23) were prepared by a film-hydration method, as described previously.[51] In detail, 10 mg of PCL_n-PEG or a mixture of 9 mg of PCL_n-PEG and 1 mg of PCL_n-PEG-Mal were dissolved in 1 mL of DCM. Next, DCM was evaporated under a nitrogen stream overnight, and a thin solid film was obtained. Subsequently, 1 mL of PBS (pH 7.4) was added to hydrate the copolymer film. The mixture was heated up to 65 °C in a water bath for 15 min and then sonicated for 2 min at 40 °C to obtain a homogeneous micellar dispersion. Next, the dispersion was equilibrated at RT for 15 min, followed by extrusion through a 0.2 μm regenerated cellulose syringe filter (Phenex). The Z-average hydrodynamic diameter (Z_{ave}) and the size distribution (polydispersity index, PDI) of the formed micelles were determined at a fixed scattering angle of 173° and 25 °C using a ZetaSizer Nano S (Malvern). The zeta potential was measured at 25 °C using a Malvern Zetasizer NanoZ (Malvern Instruments, Malvern, UK) after the formed dispersion was 10 times diluted with 10 mM HEPES buffer (pH 7.4). The critical micelle concentration (CMC) of the different micelles consisting of a mixture of 90% PCL_n-PEG and 10% PCL_n-PEG-Mal was determined with the pendant drop method as reported previously.[51] The CMCs of micelles composed of 100% PCL_n-PEG were not measured, because these micelles were not used for any of the studies described.

mTHPC-loaded micelles (different loadings) were prepared by the addition of mTHPC solution in THF (5 mg/mL, volume depending on the aimed wt % loading), to the above-mentioned polymer solution in DCM, and then, the remaining procedures were the same as mentioned above. The absorbance of diluted micelles in DMF at 651.5 nm was recorded using a UV-2450 Shimadzu spectrophotometer, and calibration was done using a series of standard solutions of mTHPC in DMF to calculate the drug loading capacity (LC) and drug loading efficiency (LE) according to the following equations.

$$\text{LC}\ (\%) = \frac{W_{ld}}{W_{ld} + W_p} * 100\%$$

$$\text{LE}\ (\%) = \frac{W_{ld}}{W_{fd}} * 100\%$$

in which W_{ld}, W_{fd}, and W_p represent the mass of loaded mTHPC in the micelles, the feeding amount of mTHPC, and the polymer mass, respectively.

2.5. EGa1 Conjugation to Polymeric Micelles. The EGFR-targeted nanobody EGa1 as described by Hofman et al.[54] was produced and purified as described in ref 55 except that a slightly shorter tag for purification and detection was used, leading to protein with a theoretical molecular weight of 17 097 Da (including the purification tag, determined using ExPASy ProtParam tool). EGa1 was modified with *N*-succinimidyl-*S*-acetylthioacetate (SATA) at a 1:5 EGa1/SATA molar ratio, followed by deacetylation to yield free thiol groups, as previously described.[55] SATA-modified lysine units in EGa1 were assessed using liquid chromatography electrospray ionization time-of-flight mass spectrometry (LC-ESI-TOF-MS) (1290 Infinity, Agilent Technologies; 6560 Ion Mobility Q-TOF LC/MS, Agilent Technologies). Ellman's assay was performed according to the manufacturer's protocol, to quantify the average number of sulfhydryl (-SH) groups per EGa1 molecule after modification with SATA, i.e., by the reaction between Ellman's reagent (5,5′-dithiobis(2-nitro-

https://dx.doi.org/10.1021/acs.molpharmaceut.9b01280
Mol. Pharmaceutics 2020, 17, 1276−1292

benzoic acid)) and free sulfhydryl groups to obtain the measurable yellow-colored product (2-nitro-5-thiobenzoic acid). Briefly, 50 μL of SATA-modified EGa1 solution and 10 μL of deprotection solution (1 M hydroxylamine hydrochloride in PBS containing 50 mM EDTA, pH 7.2) were mixed and added to 170 μL of reaction buffer (1 mM EDTA in PBS, pH 8) to which 50 μL of Ellman's reagent was added. As controls, 50 μL of native (i.e., nonmodified) EGa1 or reduced native EGa1 (obtained by incubating native EGa1 with TCEP at 1:1 molar ratio) was added to the mixture of 50 μL of Ellman's reagent and 180 μL of reaction buffer. The solutions (280 μL) were transferred into a transparent 96-well plate and incubated at RT for 15 min. Next, absorbance at 412 nm was measured using UV−vis spectroscopy (SPECTROstar Nano, BMG LabTech), and the average number of -SH groups per EGa1 nanobody was calculated using the calibration curve of a series of cysteine (Cys) solutions in reaction buffer with concentrations ranging from 4.62 to 116 nM.

For conjugation to the micelles, the deprotected EGa1/SATA was incubated with empty or mTHPC-loaded micelles (mTHPC loadings ranging from 0.5 to 10 wt %) composed of a mixture of 90 wt % PCL_n-PEG and 10 wt % PCL_n-PEG-Mal (10 mg/mL polymer concentration, prepared as described in Section 2.4) at a maleimide/EGa1 molar ratio of 100:4.5 at RT for 1 h and at 4 °C for another 12 h, allowing reaction of the introduced thiol groups in the nanobodies with maleimide groups present on the surfaces of micelles (the resulting micelles are abbreviated as EGa1-P_n micelles, n = 9, 15, or 23). This selected reaction condition was estimated to result in approximately 4.5 EGa1 molecules per micelle (assuming an aggregation number of 1000 PCL_n-PEG/PCL_n-PEG-Mal polymer chains per micelle[56,57]). After conjugation, the unreacted maleimide groups in micelles were blocked by an excess of Cys (0.33 M in PBS, 100 μL added to 2 mL micellar dispersion). Nontargeted control micelles (P_n micelles) were obtained by Cys-blocking the maleimide groups present in micelles that were not reacted with EGa1. After a 1 h reaction at RT, unconjugated EGa1 (for the targeted formulations) and Cys (for the control formulations) were removed by washing 10 times with PBS using centrifugation with Vivaspin 6 tubes (MWCO: 50 kDa for n = 9 and n = 15; 100 kDa for n = 23).

To confirm the conjugation of nanobody to micelles, sodium dodecyl sulfate-polyacrylamide gel electrophoresis (SDS-PAGE) of diluted micelles was performed. Briefly, samples were incubated with lithium dodecyl sulfate (LDS) running buffer (Bolt, Novex, Life Technologies) under reducing conditions at 80 °C for 10 min and then loaded into SDS-PAGE gel (Bolt, 4−12% Bis-Tris Plus 1.0 mm × 10 wells, Invitrogen Thermo Fisher Scientific). SDS-PAGE was performed at 80 V for about 1 h, using 2-(*N*-morpholino)-ethanesulfonic acid (MES) buffer as the electrophoretic running solution. Next, the gel was stained using the Pierce Silver Stain Kit (Thermo Fisher Scientific) following the instruction provided by Thermo Fisher Scientific. The size and zeta potential of the nanobody decorated micelles were determined as described in Section 2.4.

2.6. Cell Culture. Human epidermoid carcinoma A431 cells and human cervical carcinoma HeLa cells were obtained from the American Type Culture Collection (ATCC, Manassas, Virginia, USA). A431 and HeLa cells were cultured in Dulbecco modified eagle medium (DMEM) supplemented with glucose (1 g/L for A431 and 4.5 g/L for HeLa) and 10% (v/v) FBS. The cells were maintained at 37 °C in a humidified 5% CO_2 atmosphere. These conditions were used in all cell incubation steps described below. Both cells were grown in 75 cm^2 sterile T-flasks and passaged twice a week.

2.7. EGFR Expression by A431 and HeLa Cells. Briefly, 100 000 A431 or HeLa cells/well dispersed in DMEM containing 10% (v/v) FBS were pipetted into 96-well plates (U-bottom). After being washed with PBS containing 1% bovine serum albumin (BSA), 50 μL/well of primary antibody (mouse anti-EGFR Ab-10, 0.2 mg/mL) was added to the cells and incubated for 45 min at 4 °C. Next, the cells were washed two times with PBS containing 1% BSA, followed by the addition of secondary antibody (goat antimouse IgG-A488, 50 μL per well, 1 mg/mL). Subsequently, the 96-well plate was incubated for 30 min at 4 °C and then washed twice with 1% BSA in PBS. The mean fluorescence intensity (MFI) was measured using a flow cytometer (Canto II, BD). At least 10 000 events per sample were required. EGFR expression in A431 cells was taken as 100%.

2.8. Cell Binding and Uptake Studies. A431 and HeLa cells were used to investigate the binding and cellular uptake of EGa1-P_n micelles loaded with mTHPC (prepared as described in Section 2.5). As controls, nontargeted P_n micelles (devoid of nanobody) and EGa1-conjugated micelles coincubated with a 9-fold excess of free EGa1 (competition group) were employed.

The binding of EGa1 micelles to A431 and HeLa cells was carried out at 4 °C. In detail, A431 and HeLa cells dispersed in 100 μL of DMEM containing 10% (v/v) FBS and glucose (1 g/L for A431 and 4.5 g/L for HeLa) were seeded into 96-well plates at a density of 12 000 cells/well and allowed to adhere overnight at 37 °C and 5% CO_2. To stain nuclei, Hoechst 33342 (1:1000 dilution in PBS) was added and incubated with the cells for 30 min at 37 °C. Next, EGa1 decorated micelles or nontargeted micelles were added to the wells containing fresh medium. For the competition group, medium in wells was replaced by fresh medium, followed by the addition of an excess of free nanobody (final concentration was 0.05 mg/mL) and then immediately followed by the addition of the EGa1 micelles. Cells were incubated with the micelles (or coincubated with free EGa1) in the dark for 1 h at 4 °C. Thereafter, the cells were washed three times with PBS to remove nonbound micelles and subsequently fixed by incubating with 4% paraformaldehyde for 10 min. After removal of the paraformaldehyde solution and addition of 100 μL of PBS, confocal images were acquired on a fully automated Yokogawa High Content Imaging Platform (Model CV7000S, Yokogawa, Tokyo, Japan) equipped with a 60× water immersion objective using two channels: one channel (λ_{ex} 405 nm, λ_{em} 445 nm) for Hoechst 33342 (nuclei) and another (λ_{ex} 405 nm, λ_{em} 676 nm) for mTHPC.

The uptake of EGa1-P_n micelles by A431 and HeLa cells was studied as follows: the different formulations (EGa1 micelles, nontargeted micelles, and EGa1 micelles with free EGa1) were incubated with cells for 0.5, 1, 2, 3.5, and 7 h at 37 °C, with 5% CO_2. Hoechst 33342 (1:1000 dilution in PBS) was added 30 min before the end of the predetermined incubation period to stain the nuclei of cells. Next, DMEM-medium-containing formulations were removed from the wells and replaced by OptiMEM medium after the cells were washed three times with OptiMEM medium. Thereafter, the plates were transferred into the above-mentioned Yokogawa apparatus equipped with an incubation chamber set at 37 °C and 5%

https://dx.doi.org/10.1021/acs.molpharmaceut.9b01280
Mol. Pharmaceutics 2020, 17, 1276−1292

CO_2 and imaged using the same channels as mentioned for the cellular binding study.

For both experiments, Images were analyzed with Columbus software, and the fluorescence intensity of mTHPC was quantified by ImageJ software.

2.9. Dark and Photocytotoxicity of mTHPC-Loaded Micelles. Targeted EGa1-P_{23} micelles loaded with different mTHPC loadings (0.5 to 10% w/w) at a fixed polymer concentration (10 mg/mL in PBS) were prepared as described in Sections 2.4 and 2.5 and used to evaluate their dark toxicity and photocytotoxicity on both A431 and HeLa cells. As references, the corresponding mTHPC-loaded P_n micelles (nontargeted) and "competition group" consisting of mTHPC-loaded EGa1-P_{23} micelles and a 9-fold excess of free EGa1 were employed. As an additional comparison, free mTHPC with concentrations ranging from 0.003 to 3.8 mg/mL were prepared by diluting a 5 mg/mL mTHPC stock solution in the Foscan solvent consisting of ethanol and propylene glycol (40:60 w/w) (i.e., the solvent for its commercial formulation: Foscan). These mTHPC solutions in Foscan solvent were 50 times diluted with DMEM containing 10% v/v FBS prior to incubation with the cells.

A representative procedure to evaluate the photocytotoxicity of micellar mTHPC formulations on cells at a final polymer concentration of 1 mg/mL was the following: 6000 A431 cells/well or 5000 HeLa cells/well were seeded into 96-well plates, and after overnight culture at 37 °C and 5% CO_2, the medium in the wells was replaced by the above-mentioned mTHPC micellar dispersions (diluted 10 times in DMEM medium prior to use) with different wt % mTHPC loadings (EGa1 or nontargeted micelles) or mTHPC prepared by diluting the mTHPC solution in Foscan solvent with medium. For the competition group, medium containing free EGa1 (0.05 mg/mL) was used. The cells were subsequently incubated for 7 h in the dark, while the 2% mTHPC-loaded EGa1 micelles and corresponding controls were also incubated for 2 and 4 h. After the indicated incubation period, the media of the formulations was removed, and the cells were washed three times with DMEM medium. Next, the cells were then illuminated for 10 min with a light intensity of 3.5 mW/cm^2 (corresponding with 2.1 J/cm^2), using a homemade device consisting of 96 LED lamps (650 ± 20 nm, 1 LED per well) and then incubated with DMEM medium containing 10% (v/v) FBS overnight at 37 °C and 5% CO_2. Finally, cell viability was measured by MTS (see below).

The dark toxicity of micellar formulations on cells was determined after 7 and 24 h according to the same procedure for photocytotoxicity, except that cell viability was measured directly (without irradiation) by the MTS assay after washing off the media of the formulations.

The MTS assay was performed according to the manufacturer's instruction. In short, to each well containing 100 μL of medium including 10% (v/v) FBS to which cells adhered, 20 μL of MTS reagent was added. Subsequently, the well plate was incubated at 37 °C and 5% CO_2, and the absorbances of the different wells at 490 nm were measured with a 96-well plate reader (Biochrom EZ Read 400 Microplate reader, Biochrom, U.K.) after approximately 1 h. The viability of the cells exposed to the different micellar formulations is reported as a percentage of the viability of the untreated cells. The half maximal effective concentrations (EC_{50}) of mTHPC formulations were obtained by analysis of the cell viability data with the GraphPad Prism 7.04 software (nonlinear regression, log[inhibitor] vs normalized response).

2.10. Generation of Singlet Oxygen. Singlet Oxygen Sensor Green (SOSG, Molecular Probes) was used to evaluate the generation of singlet oxygen induced by free mTHPC and P_{23} micelles containing mTHPC. Solutions of free mTHPC and mTHPC-loaded micelles were prepared at 25 μM in Foscan solvent and PBS pH 7.4, respectively. SOSG was added to these solutions from the stock (1 mM in methanol) to obtain a final concentration of 10 μM. Control samples without mTHPC and containing 10 μM of SOSG were also prepared. Samples were transferred to a quartz cuvette and illuminated with a filtered white light source at 645−665 nm at a fluence rate of 5 mW/cm^2. During illumination, samples were stirred by placing a magnet inside the cuvette. At different time points, the cuvette was removed from the magnetic stirrer, and the fluorescence emission spectrum (λ_{exc} = 488 nm) acquired with a PerkinElmer Spectrometer LS50B (λ_{em} = 500−750 nm).

2.11. *In Vitro* Release of mTHPC-Loaded Micelles in Human Plasma. The *in vitro* release of mTHPC-loaded micelles with 5 wt % mTHPC loading (prepared in PBS as described in Section 2.4) was studied in human plasma at 37 °C, by monitoring the change of fluorescence intensity of mTHPC, as previously reported.[51] Foscan (i.e., free mTHPC solution in ethanol/propylene glycol (40:60, w/w)) was used as a reference. In short, different formulations were added to human plasma at a volume ratio of 1:9. As controls, samples were mixed with PBS or DMSO (1:9, v/v). After incubation at 37 °C, samples were taken at different time points (5 min and 0.5, 1, 1.5, 2, 3, 5, 8 h) and placed in a 384-well plate to record the fluorescence intensity using a Jasco FP8300 spectrofluorometer (Japan) at 655 nm after excitation at 420 nm.

In addition, samples of Foscan and the micellar mTHPC formulation after being incubated with human plasma (1:9, v/v) at 37 °C for 5 h were taken and diluted 1.5, 2, 4, and 30 times with either human plasma or PBS. After incubation at 37 °C, samples were taken at 0.5, 1, and 2 h and placed in a 384-well plate to record the fluorescence intensity.

2.12. *In Vivo* Pharmacokinetics. For the *in vivo* pharmacokinetic study, nontargeted P_{23} and targeted EGa1-P_{23} micelles loaded with mTHPC (0.6 wt % loading) were used and prepared as described in Sections 2.4 and 2.5, except that micelles consisted of Cy7 labeled PCL_{18}-$PDTC_{7.5}$-PEG blended with nonlabeled PCL_{23}-PEG and PCL_{23}-PEG-Mal (1.5:88.5:10, w/w/w), while free mTHPC was prepared by 2 times dilution of a stock solution of 120 μg/mL mTHPC in Foscan solvent (i.e., ethanol/propylene glycol, 40:60 w/w) with PBS (final mTHPC concentration is 60 μg/mL, corresponding to 0.6% mTHPC loading into micelles) prior to injection.

All animal experiments were approved by local and national regulatory authorities and by the local Utrecht ethics welfare committee. Female Balb/c nude mice, weighing 20−28 g, were purchased from Envigo (Horst, The Netherlands). Mice were housed in ventilated cages at 25 °C and 55% humidity under natural light/dark conditions and allowed free access to standard food and water. Mice were inoculated with 1 × 10^6 A431 cells suspended in 100 μL of PBS (pH 7.4) subcutaneously into the right flank. The experiments were performed 8−15 days later, when the A431 tumor xenograft was developed with an approximate size of 100−300 mm^3. Tumors were measured using a digital caliper. The tumor volume V (in mm^3) was calculated using the equation $V = (\pi/$

https://dx.doi.org/10.1021/acs.molpharmaceut.9b01280
Mol. Pharmaceutics 2020, 17, 1276−1292

Scheme 1. Synthesis of PCL_n-PEG and PCL_n-PEG-Mal Block Copolymers[a]

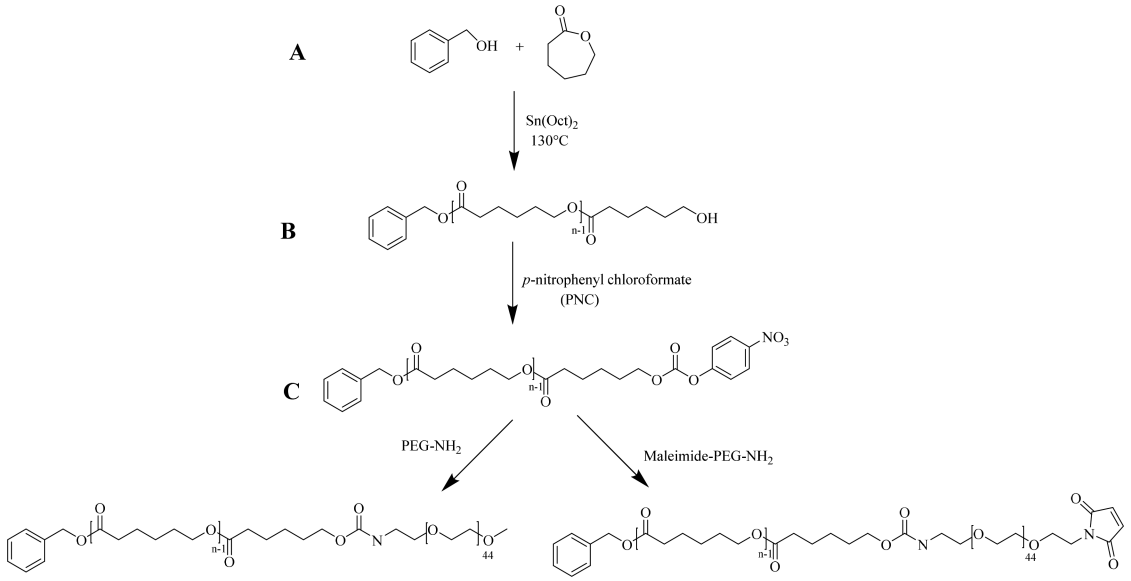

[a](A) Synthesis of PCL_n-OH by ring opening polymerization of ε-CL with benzyl alcohol. (B) Activation of the terminal hydroxyl with *p*-nitrophenyl chloroformate. (C) PCL_n-PEG/PCL_n-PEG-Mal copolymers synthesized by coupling of PEG-NH_2/Mal-PEG-NH_2 to the activated PCL oligomers.

6)LS^2 where L is the largest and S is the smallest superficial diameter.

Three groups of mice (n = 4−5 per group) were intravenously (iv) injected via the tail vein with free mTHPC and (EGa1)-P_{23} micelles in PBS at 0.6% mTHPC (w/w) loading, respectively (injection dose was 0.3 mg of mTHPC per kg of bodyweight of the mouse). Blood samples (~60 μL) were collected in tubes with EDTA-anticoagulant via a submandibular puncture from mice at 1 min and 1 and 2 h and via cardiac puncture after 4 and 24 h, post injection. Collected blood samples were centrifuged at 1000*g* for 15 min at 4 °C. To quantify the amount of Cy-7 labeled micelles, 1 volume of collected supernatant of plasma was vortex-mixed with 1 volume of PBS. The intensity of the Cy7 fluorescence of the samples (20 μL) was detected at 800 nm using an LI-COR Odyssey imaging system, and a calibration curve was prepared by a series of Cy7-maleimide solutions in the mixture of Balb/c mice plasma and PBS (1:1, v/v). To quantify the amount of mTHPC, 1 volume of collected plasma was vortex-mixed with 2 volumes of acetonitrile/ DMSO (4:1 v/v) for 1 min. The mixture was centrifuged at 15 000*g* for 10 min, and the clear supernatant was collected and analyzed by high-performance liquid chromatography (HPLC). The HPLC system consisted of a Waters X Select CSH C18 3.5 μm, 4.6 × 150 mm column with 0.1% trifluoroacetic acid in acetonitrile/water (60:40, v/v) as a mobile phase, using a flow rate of 1 mL/min. The injection volume was 20 μL, and mTHPC was detected by a fluorescence detector set at λ_{ex} = 420 nm and λ_{em} = 650 nm with a retention time of about 3 min. The measuring range was from 0.005 to 4 μg/mL and the detection limit was about 5 ng/mL. A calibration curve was obtained from a series of standard solutions of mTHPC in DMSO, to which 45 μL of Balb/c mouse plasma was added, followed by mTHPC extraction using acetonitrile/DMSO (4:1, v/v) and HPLC analysis as described above.

2.13. Statistical Analysis. Statistical analysis was done by GraphPad Prism 7.04 software. Two-way analysis of variance (ANOVA) was used to determine the significance of cellular uptake between mTHPC loaded in targeted EGa1-P_n micelles and relevant controls. Student's *t*-test was performed to determine the significance of EGFR expression between A431 and HeLa cells. A value of $p < 0.05$ was considered significant. Statistical significance is depicted as * $p < 0.05$, ** $p < 0.01$, and *** $p < 0.001$.

3. RESULTS AND DISCUSSION

3.1. Synthesis and Characterization of Copolymers. A series of PCL_n-PEG and PCL_n-PEG-Mal copolymers was synthesized by a three-step process as described previously (Scheme 1).[51] First, ring opening polymerization (ROP) of ε-CL in the melt initiated by benzyl alcohol and catalyzed by $Sn(Oct)_2$, at ε-CL/initiator molar ratios of 5.5:1, 14:1, and 23:1, respectively, was conducted to obtain the PCL_n-OH precursors with different PCL chain lengths, namely, n = 9, 15, or 23 (i.e., average numbers as calculated from ^{1}H NMR data). It is noted that the introduction of terminal aromatic rings was used to stabilize the prepared micelles by $\pi-\pi$ stacking.[58−60] Subsequently, the hydroxyl terminal groups of the different PCL_n-OH oligomers were activated by PNC and then conjugated with either PEG-NH_2 or Mal-PEG-NH_2 to yield PCL_n-PEG or PCL_n-PEG-Mal block copolymers with a carbamate linkage between the two blocks. The successful synthesis of the intermediate products and final PCL_n-PEG/PCL_n-PEG-Mal block copolymers was confirmed by ^{1}H NMR spectroscopy as described previously.[51] The characteristics of PCL oligomers and final copolymers are summarized in Table 1. This table shows that the calculated M_n values of the synthesized PCL_n oligomers and PCL_n -PEG/PCL_n-PEG-Mal block copolymers as derived by ^{1}H NMR spectroscopic analysis were very well in line with the aimed values, based on the feed ratio of monomer to initiator, except for that with the shortest CL chain length, which showed a higher M_n relative to the aimed value (actual n = 9, while the feed ratio of ε-CL to benzyl alcohol was 5.5 to 1). Taking the relatively low yield

https://dx.doi.org/10.1021/acs.molpharmaceut.9b01280
Mol. Pharmaceutics 2020, 17, 1276−1292

Table 1. Characteristics of Synthesized Intermediates and PCL_n-PEG Block Copolymers

polymer	aimed molecular weight (kDa)	^{1}H NMR M_n (kDa)	GPC M_w (kDa)	GPC M_n (kDa)	GPC M_w/M_n	yield (%)
PCL_9-OH	0.8	1.1	0.7	0.6	1.12	58
PCL_9-PNF	1.0	1.3	0.7	0.6	1.12	58
PCL_9-PEG	3.0	3.1	2.7	2.5	1.06	82
PCL_9-PEG-Mal	3.1	3.5	3.0	3.0	1.03	78
PCL_{15}-OH	1.7	1.8	1.4	1.2	1.15	81
PCL_{15}-PNF	1.9	2.0	1.3	1.2	1.15	73
PCL_{15}-PEG	3.7	3.8	3.3	3.0	1.09	56
PCL_{15}-PEG-Mal	3.8	4.1	5.4	4.6	1.18	24
PCL_{23}-OH	2.7	2.7	2.1	1.8	1.12	82
PCL_{23}-PNF	2.9	2.9	2.0	1.9	1.10	76
PCL_{23}-PEG	4.7	4.7	3.7	3.2	1.16	57
PCL_{23}-PEG-Mal	4.8	5.1	5.8	4.1	1.40	74
PEG-NH_2	n.a.[a]	2.0	1.7	1.6	1.02	n.a.[a]
Mal-PEG-NH_2	n.a.[a]	2.6	2.0	2.0	1.02	n.a.[a]

[a]n.a. = not applicable.

(58%) of PCL_9-OH into account as compared to the larger PCL_n-OH (yields >81%), this is most likely attributed to the loss of oligomers with the shortest PCL chains during the purification process. ^{1}H NMR spectra of PCL_n-PEG/PCL_n-PEG-Mal block copolymers (shown in Figure S1) show that the integral ratio of the CH_2 from benzyl alcohol at 5.11 ppm to ethylene oxide units from PEG at 3.64 ppm was about 1:110, which is close to the theoretical ratio (1:95), demonstrating that almost all PCL oligomers were equipped with a PEG chain. It is noted that ^{1}H NMR spectra of PCL_n-PEG-Mal copolymers displayed a peak at 6.70 ppm that can be ascribed to maleimide protons with the integral ratio of 1:1 compared to CH_2 from benzyl alcohol at 5.11 ppm for the three different oligomers (Figure S1), which demonstrates that all polymer chains have one terminal maleimide group. The presence of maleimide groups on PCL_n-PEG-Mal was also confirmed by the appearance of an absorbance at 293 nm in the UV−vis spectra of the polymers, which is also present in the Mal-PEG-NH_2 but absent in the UV−vis spectra of PEG-NH_2 and PCL_n-PEG (see Figure S2A). Using calibration with Mal-PEG-NH_2 (see Figure S2B), it is calculated that all polymer chains carry a maleimide group, which is in agreement with ^{1}H NMR analysis. Moreover, GPC analysis shows low polydispersity of the synthesized polymers (M_w/M_n < 1.4) with a shift of M_n with approximately 2 kDa as compared to the corresponding PCL oligomers, e.g, 2.5 kDa of PCL_9-PEG vs 0.6 kDa of PCL_9 -OH (representative GPC graphs shown in Figure S3; all the GPC data is summarized in Table 1). The peak shift indicates that indeed PCL_n-PEG/PCL_n-PEG-Mal block copolymers rather than a physical mixture of PCL oligomers and PEG were formed.

In addition, to label the PCL_{23}-PEG based polymer with the near-infrared (NIR) fluorophore Cy7 for *in vivo* pharmacokinetic study, DTC units containing disulfide bonds were introduced to PCL-PEG by ROP of CL and DTC (Scheme S1). Subsequently, the disulfide bonds in the resulting PCL_{18}-$PDTC_{7.5}$-PEG were reduced to free thiols by a reducing agent (i.e., TCEP), which reacted with Cy7-maleimide via the thiol-maleimide reaction (Scheme S1). After the coupling reactions with a coupling efficiency of 17% (calculated based on the calibration curve of Figure S4A), on average, one polymer chain carried 0.17 Cy7 labels. GPC chromatograms (Figure S4B) of the Cy7 labeled polymer showed the successful coupling of Cy7 with the polymer with negligible free Cy7 present in the resulting Cy7 labeled polymer.

3.2. Preparation of Polymeric Micelles. Micelles composed of PCL_n-PEG and 9:1 mixtures of PCL_n-PEG and PCL_n-PEG-Mal (n = 9, 15, and 23) at a polymer concentration of 10 mg/mL were prepared by a film-hydration method (Scheme 2). Table 2 shows that micelles with or without PCL_n-PEG-Mal had small hydrodynamic diameters (ranging from 17−45 nm, with increasing PCL chain length) and a near neutral zeta potential, suggesting that the addition of PCL_n-PEG-Mal had no effect on the characteristics of the micelles. The CMCs of the micelles composed of 90% PCL_n-PEG and 10% PCL_n-PEG-Mal were in the range of previously published data on PCL-PEG.[51]

3.3. EGa1 Modification and Its Conjugation to Polymeric Micelles. EGa1 was produced and purified as described in ref 55 and characterized by LC-ESI-TOF-MS (Figure S5A). A major peak with an m/z value at 17 096 Da was detected, in agreement with the theoretical mass of this protein. The EGa1 nanobody was modified using 5 equiv of SATA reagent that can react with the six primary amines of the EGa1 protein (five lysine amino acids and one at the N-terminal). The successful modification was demonstrated using

Scheme 2. Preparation of Polymeric Micelles Conjugated with EGa1 (Targeted) or Cys (Nontargeted)

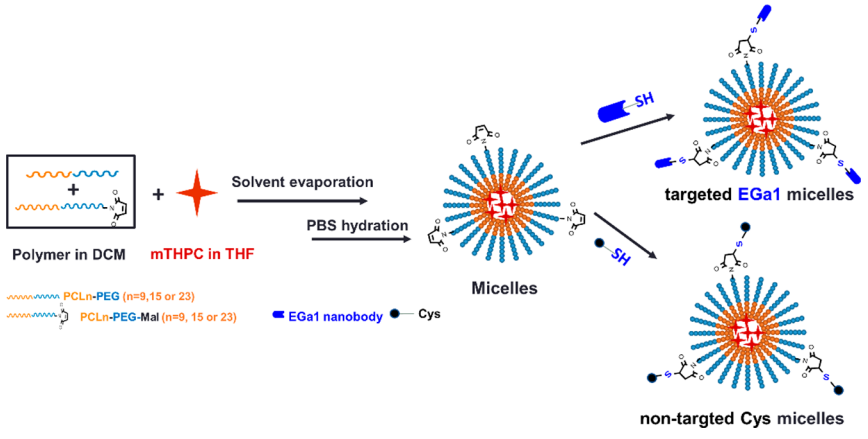

https://dx.doi.org/10.1021/acs.molpharmaceut.9b01280
Mol. Pharmaceutics 2020, 17, 1276−1292

Table 2. Characteristics of Micelles Composed of PCL_n-PEG and 9:1 (w/w) Mixtures of PCL_n-PEG and PCL_n-PEG-Mal

polymer(s)	Z_{Ave} diameter (nm)[a]	PDI[a]	ζ-potential (mV)[a]	CMC (mg/mL)
PCL_9-PEG	17 ± 1	0.07 ± 0.02	−2.3 ± 0.0	0.04[51]
PCL_9-PEG/PCL_9-PEG-Mal	17 ± 1	0.09 ± 0.01	−2.3 ± 0.0	0.06
PCL_{15}-PEG	25 ± 2	0.20 ± 0.01	−1.9 ± 0.1	n.d.[b]
PCL_{15}-PEG/PCL_{15}-PEG-Mal	26 ± 3	0.20 ± 0.02	−2.0 ± 0.3	0.05
PCL_{23}-PEG	43 ± 2	0.20 ± 0.01	−1.9 ± 0.4	n.d.[b]
PCL_{23}-PEG/PCL_{23}-PEG-Mal	45 ± 4	0.15 ± 0.03	−2.2 ± 0.2	0.02

[a]Data were obtained from three independently prepared batches. [b]n.d. = not determined.

Table 3. Characteristics of EGa1 and Cys Decorated Micelles[a] Composed of 9:1 Mixtures of PCL_n-PEG and PCL_n-PEG-Mal

				5 wt % feed		0.5 wt % feed	
polymer	conjugated agent	Z_{Ave} diameter (nm)	ζ-potential (mV)	LE%[b]	LC%[b]	LE%[b]	LC%[b]
PCL_9-PEG/PCL_9-PEG-Mal	Cys	17 ± 1	−5.0 ± 0.7	64	3.2	65	0.3
	EGa1	18 ± 1	−6.2 ± 1.5	64	3.2	65	0.3
PCL_{15}-PEG/PCL_{15}-PEG-Mal	Cys	25 ± 3	−4.1 ± 0.7	53	2.8	65	0.3
	EGa1	27 ± 2	−5.5 ± 1.1	53	2.8	65	0.3
PCL_{23}-PEG/PCL_{23}-PEG-Mal	Cys	43 ± 3	−4.8 ± 0.2	54	2.8	70	0.3
	EGa1	45 ± 5	−5.2 ± 0.7	54	2.8	70	0.3

[a]Targeted EGa1-P_n and nontargeted P_n micelles. [b]SD ≤ 1%.

LC-ESI-TOF-MS analysis (Figure S5B), which clearly showed two peaks with m/z values corresponding to modification with one and two SATA units (mass: 116 Da) in the deconvoluted mass spectrum. Ellman's assay was carried out to quantify the average number of thiol groups present on the EGa1 nanobody after deprotection of the SATA. The results show (Figure S5C) that reaction of EGa1 with SATA at a molar ratio of 1:5 led to approximately two sulfhydryl groups introduced per protein molecule. As controls, Ellman's assay on native (nonmodified) EGa1 and reduced EGa1 (i.e., with one split disulfide bond) showed on average 0.19 and 1.93 thiols, respectively, as expected.

Micelles consisting of 9:1 mixtures of PCL_n-PEG and PCL_n-PEG-Mal (n = 9, 15, and 23) were reacted with either Cys or deprotected EGa1-SATA to obtain nontargeted P_n and targeted EGa1-P_n micelles, respectively (Scheme 2). DLS shows that the sizes of P_n and EGa1-P_n micelles (Table 3) were comparable to those of the native micelles (Table 2), but the former had a slightly more negative surface charge at pH 7.4 (−4 to −6 mV for P_n micelles decorated with Cys or EGa1 vs around −2 mV for native micelles), which can be explained by the presence of the negatively charged nanobody at pH 7.4 (theoretical pI ≈ 6.6, according to ExPASy ProtParam tool) at the surfaces of the micelles. UV−vis detection shows that mTHPC was quite efficiently (50−70%) encapsulated inside particle cores at different feeds (see Table 3).

To establish whether EGa1 was indeed covalently linked to the polymeric micelles and not physically adsorbed, an SDS-PAGE assay of the samples was performed (Figure 1). For all the three conjugated micelles, one band located at a slightly higher molecular weight than the EGa1 band appeared, as a result of the conjugation of EGa1 with one PCL_n-PEG-Mal polymer chain. A second band near 30 kDa appeared as well, most likely representing two PCL_n-PEG-Mal polymer chains conjugated to an EGa1 molecule due to the presence of more than one SATA modification on the nanobody. These two bands were not observed in the samples of micelles alone and micelles incubated with nonreactive (i.e., not deprotected) EGa1-SATA, further convincingly demonstrating successful conjugation of EGa1 to the micelles (see Figure S6). The band

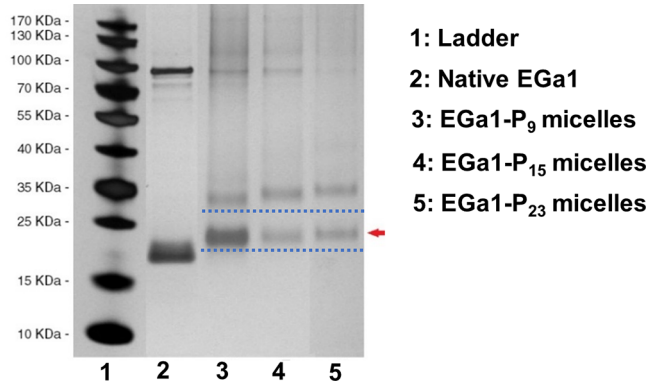

Figure 1. SDS-PAGE silver staining of mTHPC-loaded EGa1-conjugated micelles (EGa1-P_n micelles) obtained after 10 washes with PBS following the overnight conjugation of micelles with deprotected EGa1-SATA. Native EGa1 was used as a control. The red arrow indicates a band of EGa1 with one polymer chain conjugated.

of the unconjugated EGa1 was not detected in the micellar samples, confirming its full removal through Vivaspin washes (Figure 1).

3.4. Cell Binding and Uptake Studies. The cell binding capacity of EGa1 decorated micelles was studied with binding assays at 4 °C, at which cell transport processes (e.g., internalization) are markedly reduced, using two cell lines differing in EGFR expression level: A431 cells express 90% more EGFR compared to HeLa cells, as indicated by flow cytometry (Figure S7). For this, the intrinsic fluorescence of mTHPC was detected using confocal microscopy. Figure 2A shows the fluorescence intensity associated with A431 and HeLa cells after 1 h of incubation of mTHPC-loaded EGa1-P_n micelles (n = 9, 15, or 23) and relevant controls at 4 °C. EGa1-P_{15} and EGa1-P_{23} micelles clearly had extensive interaction with the membrane of A431 cells. However, cell association was less visible for the EGa1-P_9 micelles. This might be due to destabilization of these micelles as previously observed[51] or a particle size (around 15 nm) that is too small to promote multivalent binding with the receptor.[26,45,48] For all the

https://dx.doi.org/10.1021/acs.molpharmaceut.9b01280
Mol. Pharmaceutics 2020, 17, 1276−1292

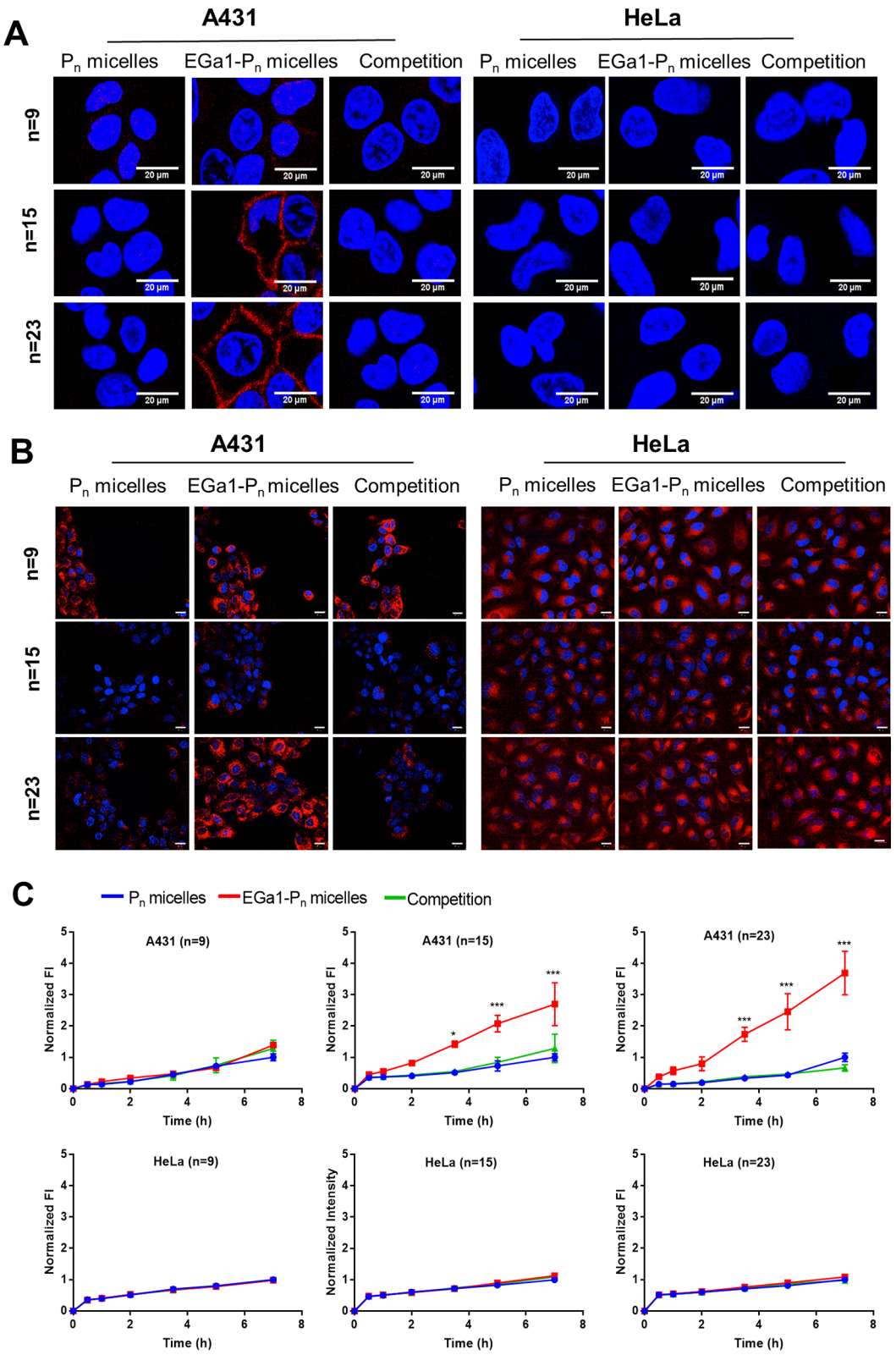

Figure 2. (A,B) Representative confocal fluorescence microscopic images of A431 and HeLa cells incubated with mTHPC-loaded micelles of three tested groups: P_n micelles (nontargeted), EGa1-P_n micelles (targeted), and a competition group composed of EGa1-P_n micelles coincubated with a 9-fold excess of free EGa1, respectively (n = 9, 15, 23; 5 wt % mTHPC loading used for micelles with n = 9 and 15 and 10 wt % mTHPC loading used for micelles with n = 23). Cells were incubated for 1 h at 4 °C (A) and for 7 h at 37 °C (B). Cell nuclei were stained in blue with Hoechst, while the fluorescence of mTHPC is presented in red. Scale bars indicate 20 μm. Excitation times applied for obtaining these confocal images were 50 ms for A431 cells and 100 ms for HeLa cells. (C) Quantification of fluorescence intensity of mTHPC (λ_{ex} 405 nm, λ_{em} 676 nm) of A431 and HeLa cells incubated with micellar formulations. The quantified fluorescence intensity was normalized by the intensity of P_n micelles after 7 h of incubation in each group and by the number of cells.

https://dx.doi.org/10.1021/acs.molpharmaceut.9b01280
Mol. Pharmaceutics 2020, 17, 1276−1292

nontargeted controls (P_n micelles), association with A431 cells was not observed. In addition, the binding observed for EGa1-P_{15} and EGa1-P_{23} micelles was absent in groups containing an excess of free EGa1, suggesting that the free EGa1 blocked the interaction of EGa1-conjugated micelles with EGFR on the surfaces of A431 cells. Also, fluorescence of mTHPC was not detected for low-EGFR-expressing HeLa cells for any of the formulations. These results indeed confirm that the EGa1 decorated micelles bind to the EGFR receptor on A431 cells, which also implies that conjugation of EGa1 to the micelles did not adversely affect the binding capability of the nanobody for its target.

To investigate the cellular internalization of the different formulations, mTHPC-loaded EGa1-P_n micelles, their controls (nontargeted P_n micelles and competition group), as well as free mTHPC were incubated with A431 and HeLa cells for different time points between 0.5 and 7 h at 37 °C. The representative microscopic images show that regarding the low-EGFR-expressing HeLa cells, only low fluorescence was visible after longer excitation times, as compared to the excitation times employed to image A431 cells (100 vs 50 ms, respectively), and no selectivity was observed between the different micelles (Figure 2B). In strong contrast, a substantial increase in fluorescence intensity of mTHPC for A431 cells after 7 h of incubation with mTHPC-loaded targeted EGa1-P_{15} and EGa1-P_{23} micelles was observed, as compared to their nontargeted controls. Furthermore, uptake of these micelles was blocked by an excess of free EGa1 (Figure 2B), which implies that mTHPC is indeed taken up in the micellar form through these EGa1-P_{15} and EGa1-P_{23} micelles. Concerning the EGa1-P_9 micelles incubated with A431 cells, no difference in fluorescence intensity was observed compared to relevant controls, which is consistent with the binding study. This suggests that the small size (around 15 nm) of these micelles may cause uptake through other mechanisms rather than receptor binding followed by endocytosis[26,45,48] or that this nonspecific uptake is caused by released mTHPC from these (less stable) micelles.[51] Indeed, free mTHPC showed efficient uptake by A431 cells (Figure S8). The fluorescence signal of mTHPC, regardless of the used formulations, was predominantly located in the perinuclear regions rather than on the cell surface, which is in good agreement with previous studies of a liposomal (Foslip) and a micellar formulation.[51,61,62] mTHPC in its free form was taken up efficiently by both A431 and HeLa cell lines at a similar level, as can be noticed from Figure S8, where stronger fluorescence was observed with even shorter excitation times than that used for imaging the micellar formulations. This confirms the known nonselective uptake of free mTHPC, which when compared to the uptake observed for the micellar formulations (Figure S8 vs Figure 2B) demonstrates the possibility to enable selective uptake using EGa1-targeted micelles, as described in the present study.

Although differences in fluorescence intensity are observed between the uptake of free mTHPC and micellar formulations containing the same dose of mTHPC (for instance, Figure 2B vs Figure S8A), comparisons between these are difficult as the lower uptake of micellar formulations could occur due to its PEG corona,[63,64] and the mTHPC fluorescence is likely quenched in the micelles at such high PS loading (≥5 wt %).[51] In respect of the micellar formulations, even if the fluorescence of mTHPC is (differently) quenched inside the micelles, each group (P_n, n = 9, 15, and 23) has the same amount of mTHPC loaded; thus, comparisons of the fluorescence intensity are possible within the targeted, nontargeted, and the competition groups (Figure 2B,C).

The quantified fluorescence intensity from the images (Figure 2C) indicates that the micelles showed a time-dependent increasing cellular uptake of fluorescent mTHPC by both A431 and HeLa cells. Most importantly, cellular uptake of mTHPC-loaded targeted EGa1-P_{15} and EGa1-P_{23} micelles by A431 cells showed a statistically significant difference (i.e., 3−4 times higher after 7 h) as compared to nontargeted P_{15} and P_{23} micelles (red vs blue lines in Figure 2C). Most significant enhancement of cellular uptake as observed for EGa1-P_{23} micelles relative to EGa1-P_{15} micelles might be due to their excellent size (∼45 nm), since it has been shown in previous studies that 40−50 nm nanoparticles are optimal for receptor-mediated internalization.[45,48] Notably, the uptake by A431 cells can be blocked or prevented, by the coincubation of EGa1 decorated micelles with an excess of free nanobody (Figure 2C, green curves). Meanwhile, no difference was observed in cellular uptake by HeLa cells for the different formulations (Figure 2C), confirming that the uptake of the micelles by A431 cells is EGFR-mediated. Cellular uptake of mTHPC-loaded P_9 based micelles was similar for all three groups, and no beneficial effects of EGa1 decoration were observed as was also concluded from earlier images (Figure 2B) and is in agreement with the nondetected cell association of mTHPC in the binding assay performed at 4 °C (Figure 2A). As mentioned before, this could be caused by the premature release of mTHPC from the micelles due to their instability[51] or other uptake mechanisms.[26,45,48] Altogether, these results confirm that the EGa1-P_{15} and EGa1-P_{23} micelles can selectively deliver mTHPC inside EGFR-overexpressed cells due to receptor-mediated cellular uptake.

3.5. Dark and Photocytotoxicity of mTHPC-Loaded Micelles. The cytotoxicity assessment of empty micelles (Figure S9) shows that, regardless of EGa1 conjugation, they all have an excellent cytocompatibility, since no toxic effects were observed at 2 and 4 mg/mL. The *in vitro* dark and photocytotoxicity experiments were only carried out with mTHPC-loaded P_{23} and EGa1-P_{23} micelles, because these micelles showed the highest cellular uptake by A431 cells (Figure 2C) as compared to P_{15} micelles. Therefore, EGa1-P_{23} and P_{23} micelles with different mTHPC loadings were prepared (the actual LE% values are shown in Tables 3 and S1, and confirmation of successful EGa1 conjugation is shown in Figure S10). The toxicity of the micellar formulations was compared with that of free PS at the same concentrations.

As shown in Figure 3 (green, red, and blue lines), the different micellar PS formulations, including the one with the highest mTHPC loading of 76 μg/mL (corresponding to 10 wt % feed loading in micelles) showed no cytotoxicity on A431 and HeLa cells after incubation with cells in the dark for 7 and 24 h, irrespective of EGa1 presence. On the other hand, cells incubated with free mTHPC (medium also containing 2% ethanol/propylene glycol (40:60 w/w) solvent) displayed a dose- and time-dependent decrease of cell viability, suggesting the toxicity of free mTHPC occurred even without illumination at mTHPC concentrations higher than 50 μg/mL after 7 h and 20 μg/mL after 24 h (Figure 3, black and gray lines), respectively. It is worth mentioning that ethanol/propylene glycol solvent present in the cultural medium was not toxic for A431 and HeLa cells in the concentration range tested, suggesting that the observed toxicity of mTHPC is not ascribed to the used solubilization vehicle. Depending on the

https://dx.doi.org/10.1021/acs.molpharmaceut.9b01280
Mol. Pharmaceutics 2020, 17, 1276−1292

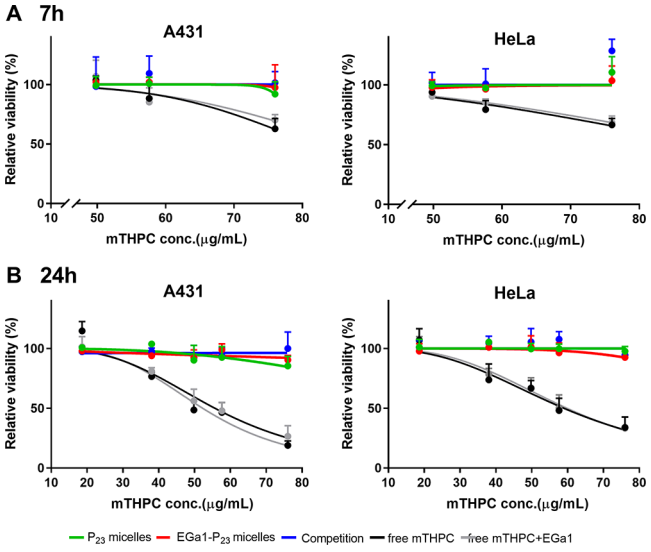

Figure 3. Dark toxicity established using MTS assay of free mTHPC and mTHPC loaded in P_{23} or EGa1-P_{23} micelles (at 1 mg/mL polymer) at varying mTHPC loadings on A431 and HeLa cells after 7 (A) and 24 h (B). In the legend, "competition" represents mTHPC loaded in EGa1-P_{23} micelles coincubated with free EGa1, while "free mTHPC+EGa1" indicates free mTHPC coincubated with free EGa1.

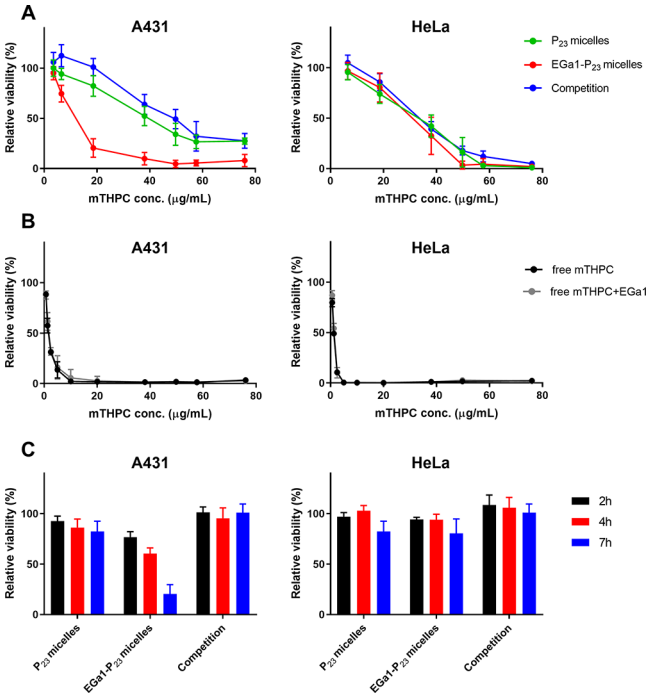

Figure 4. (A,B) Dose-dependent photocytotoxicity (MTS assay) on A431 and HeLa cells after 7 h of preincubation with mTHPC loaded in P_{23} micelles (nontargeted) or EGa1-P_{23} micelles (targeted) composed of 1 mg/mL polymer and varying mTHPC loadings (A) or free mTHPC (B). (C) Time-dependent photocytotoxicity (MTS assay) on A431 and HeLa cells preincubated with mTHPC loaded in P_{23} and EGa1-P_{23} micelles (1 mg/mL polymer and 18.6 μg/mL mTHPC (corresponding to ∼2 wt % mTHPC loading)). After the reported preincubation periods and washings, the cells were illuminated for 10 min at 3.5 mW/cm^2. In the legend, "competition" in (A) and (C) represents mTHPC loaded in EGa1-P_{23} micelles and coincubated with a 9-fold excess of free EGa1, while "Free mTHPC +EGa1" in (B) indicates free mTHPC coincubated with a 9-fold excess of free EGa1.

cell type used and incubation time, dark toxicity of free mTHPC at concentrations between 2.5 and 100 μg/mL was also found in other studies.[62,65] Interestingly, these results imply that cytotoxicity of mTHPC in the absence of light could markedly be reduced by the formulation in micelles, especially for the long incubation period, as shown previously also for its liposomal formulation (i.e., Foslip).[65]

The photocytotoxicity of mTHPC loaded in P_{23} micelles with or without EGa1 decoration toward A431 and HeLa cells was studied with various mTHPC concentrations at a fixed polymer concentration (1 mg/mL; far above the CMC of 0.02 mg/mL (see Table 2)), by illuminating the cells with 3.5 mW/cm^2 for 10 min after 7 h of preincubation with the different PS formulations. Figure 4A shows that for A431 cells, mTHPC-loaded micelles decorated with EGa1 nanobody (red line) had a significantly lower EC_{50} value (10 μg/mL) than the nontargeted micelles and competition group (EGa1 micelles plus free EGa1) (38 and 48 μg/mL, respectively, see Table S2), demonstrating increased photocytotoxicity for the targeted micelles, which is most likely attributed to the higher extent of internalization resulting from EGa1 targeting (as shown in Figure 2C). No selective photocytotoxicity was seen in HeLa cells, neither with EGa1-P_{23} micelles nor with their controls (nontarget and competition groups). As expected, no selective killing capacity of A431 and HeLa cells was shown by free mTHPC, whether coincubated with free EGa1 or not (Figure 4B). It is worth noting that the EC_{50} value of free mTHPC on A431 (∼1.6 μg/mL) (calculated from Figure 4B, shown in Table S2) was lower than the best performing EGa1 decorated micellar formulation (10 μg/mL mTHPC), probably related to the higher internalization rate of free mTHPC or a different intracellular distribution, which may affect singlet oxygen production or its efficacy.[51] In that respect, although it is difficult to predict what happens inside cells, we could confirm that mTHPC can still lead to generation of singlet oxygen when loaded inside micelles (Figure S11).

Importantly, at a polymer concentration of 1 mg/mL, the photocytotoxicity of mTHPC loaded in EGa1-P_{23} micelles was 3 times higher for A431 cells than for HeLa cells (EC_{50} of approximately 10 μg/mL mTHPC for A431 vs about 30 μg/mL mTHPC for HeLa, see Table S2), suggesting effective selectivity in terms of photocytotoxicity between A431 and HeLa cells. This selectivity in photoinduced cell killing is most interesting for achieving the targeted PDT to EGFR-over-expressing cancers.

To investigate the effect of the incubation time on photocytotoxicity, the cells were illuminated after incubation for 2, 4, and 7 h with mTHPC-loaded EGa1-P_{23} micellar formulations consisting of 1 mg/mL polymer and 18.6 μg/mL mTHPC (corresponding to ∼2 wt % loading). Figure 4C shows that only A431 cells incubated with mTHPC loaded in targeted EGa1-P_{23} micelles showed a decrease of cell viability over time (i.e., time-dependent cell death), whereas hardly any (time-dependent) photocytotoxicity was observed at this concentration of mTHPC loaded in nontargeted micellar PS formulations, its competitive control on A431 cells, and for all formulations on HeLa cells (see also in Figure 4A). These results are in good agreement with cellular uptake observations, in which we showed that EGa1-conjugated micelles were taken up to a higher extent than their controls by A431 cells (see Figure 2C). This indicates that the selective internal-

https://dx.doi.org/10.1021/acs.molpharmaceut.9b01280
Mol. Pharmaceutics 2020, 17, 1276−1292

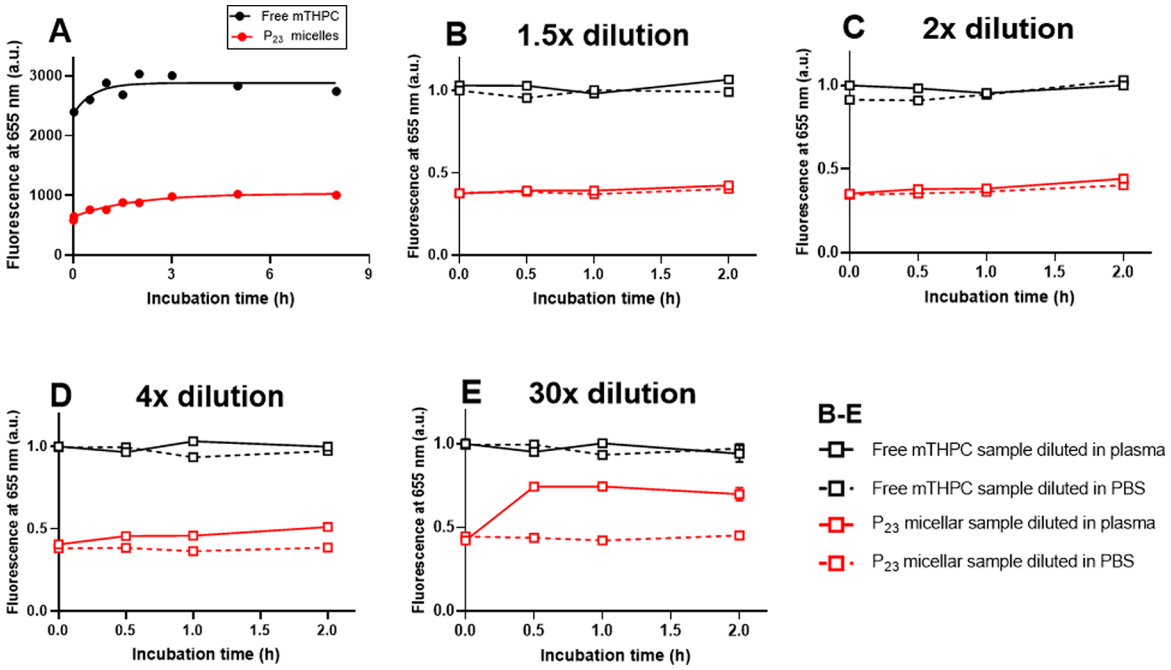

Figure 5. (A) Fluorescence intensity of free mTHPC (i.e., Foscan) and mTHPC loaded in P_{23} micelles at a final mTHPC concentration of 40 μg/mL (corresponding to 5 wt % mTHPC loading in micelles) in human plasma as a function of time; Foscan and mTHPC-loaded micelles were 10× diluted with full plasma and incubated, while the mTHPC fluorescence was recorded at 37 °C over a period of 8 h. The fluorescence intensities of the corresponding mTHPC-loaded micelles diluted with PBS were used as 0 h time point. (B–E) Fluorescence intensity of free mTHPC and mTHPC-loaded P_{23} micelles in human plasma as a function of time after dilution, normalized by the intensity of the corresponding free mTHPC samples upon dilution with human plasma at 0 h; free mTHPC and mTHPC-loaded micelles were preincubated with human plasma (1:9, v/v) at 37 °C for 5 h and then further diluted 1.5, 2, 4, or 30× with human plasma or PBS and further incubated, while the mTHPC fluorescence was recorded at 37 °C over a period of 2 h. The fluorescence intensities of mTHPC in different formulations recorded right after dilution were used as the 0 h time points.

ization of the PS-loaded micelles has a major contribution to cell killing (i.e., photocytotoxicity).

It is worth mentioning that other types of targeting ligands, such as folate and RGD peptide, have also been investigated for the targeted intracellular delivery of mTHPC in various cancer cells.[66−69] For example, Moret et al. showed that mTHPC encapsulated in folate-targeted PEGylated liposomes (i.e., folate-targeted FosPEG) exhibited enhancement of internalization and photoinduced cytotoxicity of mTHPC, by maxima of 2-fold and 1.5-fold, respectively, as compared to nontargeted liposomes, in folate-receptor-positive KB cells.[67] However, a previous study on transferrin-receptor-targeted FosPEG displayed that as compared to unmodified liposomes, transferrin-conjugated FosPEG did not improve the intracellular accumulation and the photocytotoxicity of mTHPC in transferrin-receptor-abundant OE21 cancer cells.[69] In contrast, P_{23} micelles decorated with the EGa1 nanobody used in our work exhibited a significant improvement of internalization and photocytotoxicity of mTHPC on EGFR-overexpressing A431 cells, by 4 times after 7 h of incubation (Figures 2C and 4A), as compared to the nontargeted micelles, indicating that our system has improved selectivity over the aforementioned liposomes. Our study indeed exemplifies that furnishing a targeting ligand, namely a nanobody, on nanoparticles is an attractive strategy for improving selectivity and efficacy of PDT *in vivo*.

3.6. *In Vitro* Release of mTHPC from Micelles in Human Plasma. Before investigating these micelles *in vivo*, we first investigated the *in vitro* release of mTHPC loaded in the best P_{23} micelles in human plasma over time at 37 °C (Figure 5) and compared this with Foscan (free mTHPC in solvent). Human plasma was selected, because it is biologically more relevant than a saline solution would be; however, this renders quantification of the released mTHPC difficult due to the small dimensions of the micelles that are difficult to separate from plasma proteins or lipoproteins that may contain released mTHPC. Therefore, for this stability study, we made use of the quenched state of the fluorescence resulting from the high-mTHPC local concentration inside the micellar core.[51] Release of mTHPC from the micelles should decrease mTHPC local concentration inside the micelles, thus decreasing quenching and increasing the fluorescence intensity. Similarly as observed in our previous study,[51] the fluorescence of mTHPC-loaded micelles upon 10× dilution in PBS was low due to fluorescence quenching, though stable in time over 8 h at 37 °C (Figure S12A). In contrast, upon 10× dilution in DMSO, the fluorescence of mTHPC-loaded micelles was restored to the same level as free mTHPC, suggesting the dequenching of mTHPC due to the destruction of micelles by DMSO (Figure S12B). Upon 10× dilution in plasma, Foscan gave stable fluorescence at a value of ∼2800 a.u. after 30 min of incubation (Figure 5, black line). For the micellar mTHPC formulation, the fluorescence of mTHPC increased slightly within the first 3 h of incubation and then leveled off at ∼1000 a.u. (Figure 5A, red line), which was significantly lower than that of free mTHPC (2800 a.u.). This result suggests that despite a slight initial release of mTHPC in the first 3 h, the majority of mTHPC was sufficiently retained in micelles in the presence of plasma for at least 8 h.

https://dx.doi.org/10.1021/acs.molpharmaceut.9b01280
Mol. Pharmaceutics 2020, 17, 1276−1292

To reveal whether the release of mTHPC from micelles is dependent on the ratio between micelles and plasma, mTHPC-loaded P_{23} micelles after incubation with human plasma for 5 h were further diluted with human plasma or PBS in different proportions. As a comparison, free mTHPC samples were treated under the same conditions. When the micelles preincubated with plasma were diluted with PBS, the fluorescence of mTHPC that was released from the micelles was kept constant in time (Figure 5B–E, broken red lines) and remained lower than that of diluted free mTHPC. Upon 1.5× and 2× dilution of the plasma containing micelles instead of PBS, fluorescence of mTHPC remained stable and comparable to that observed when it was diluted in PBS (Figure 5B,C, solid red lines). With a further increase of the dilution factor in plasma to 4 times, fluorescence of mTHPC in micelles only slightly increased during the first 1 h of incubation and then leveled off (Figure 5D, solid red line). Surprisingly, the plateau fluorescence levels upon 1.5 to 4× dilution in plasma were much lower than that observed from the corresponding free mTHPC samples (Figure 5B–D, black lines), suggesting sufficient mTHPC retention in micelles in the presence of up to 40 times plasma (v/v). Even upon a large dilution in plasma up to 30× (final polymer concentration: 0.03 mg/mL, close to CMC of 0.02 mg/mL, Table 2), a lower fluorescence level of the micellar mTHPC formulation was observed than of free mTHPC samples (Figure 5E). These results suggest that some extent of mTHPC can be retained in P_{23} micelles in the presence of the large amount of plasma (300 times, v/v).

3.7. *In Vivo* Pharmacokinetics of mTHPC and Micelles.

For successfully translating the *in vitro* selectivity of PDT into the *in vivo* situation, the prerequisite is prolonged circulation of nanocarriers. Therefore, the pharmacokinetic profiles of free mTHPC, Cy7 labeled P_{23}, and EGa1-P_{23} micelles loaded with mTHPC were studied in mice bearing human A431 tumor xenografts. Figure 6 shows that the incorporated mTHPC in

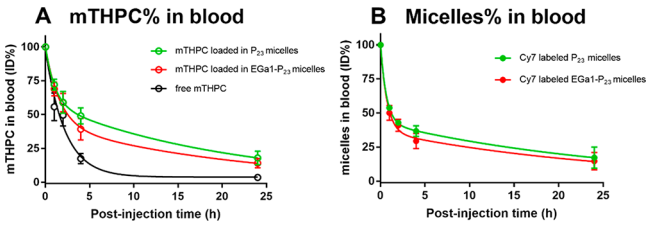

Figure 6. *In vivo* pharmacokinetics of free mTHPC (A) and Cy7 labeled (EGa1)-P_{23} micelles (B) loaded with mTHPC (A) upon tail vein administration in A431 tumor-bearing Balb/c mice (0.3 mg of mTHPC per kg of bodyweight of the mouse, i.e., ∼6 μg of mTHPC). Blood samples taken at different time points were used to quantify the percentage of mTHPC and the corresponding Cy7 labeled micelles of the injected dose (%ID) present in systemic circulation. Data are presented as mean ± SD, $N = 4$.

micellar formulations and the corresponding micelles, regardless of being decorated with EGa1 or not, displayed similar clearance profiles (red and green line), suggesting that conjugated nanobody had a minor influence on the clearance of these micelles. More importantly, mTHPC in these micelles clearly showed slower elimination kinetics from the blood circulation than free mTHPC (Figure 6A, red and green lines vs black line) and also than when mTHPC was loaded into previously reported P_9 micelles,[51] particularly 4 h post injection (∼45% for mTHPC in (EGa1)-P_{23} micelles vs ∼17% for mTHPC in its free form and P_9 micelles of the injected dose (ID) detected in blood). According to the semilogarithmic plot (Figure S13), these data can be fitted by a two-phase decay model, which was also previously applied for liposomal mTHPC formulations and Foscan.[15,70,71] The thus calculated pharmacokinetic parameters (Table 4) show two

Table 4. Half-Life and the Area under the Curve (AUC) Values of Free mTHPC, mTHPC Loaded in Micelles, and the Corresponding (Cy7 Labeled) Micelles

		half-life (h)		AUC (h*%)	
detection	formulations	phase α	phase β	phase α	phase β
mTHPC	free mTHPC	0.04	2.1	77	278
	mTHPC in EGa1-P_{23} micelles	1.1	14.8	147	631
	mTHPC in P_{23} micelles	0.7	14.1	150	778
Cy7	EGa1-P_{23} micelles	0.5	18.3	124	513
	P_{23} micelles	0.5	18.1	119	620

elimination half-lives and the area under the curve (AUC) values that characterize the pharmacokinetics of mTHPC and micelles. The half-lives of the alpha phase for mTHPC in micellar formulations, ranging from 0.7 to 1 h, were similar to that observed for the corresponding micelles (0.5 h). In line with this, AUC values, reflecting drug concentrations in plasma, of the incorporated mTHPC and its corresponding micelles in this phase were also comparable (Table 4). The half-life and AUC values of the beta phase for both the incorporated mTHPC and the corresponding micelles were considerably larger than the alpha phase. However, although both showed similar AUC values, the half-lives of mTHPC in micelles in the beta phase were obviously shorter than those of the corresponding micelles (∼14 vs ∼18 h, Table 4), indicating that mTHPC is released at least partly from the micelles prior to being removed from the blood. This premature cargo release was also observed previously in various liposomal mTHPC formulations and other drug-loaded nanocarriers.[71,72] Surprisingly, although the incorporated mTHPC in our micelles showed slightly shorter half-lives of the beta phase than when encapsulated in the liposome (14 vs 18 h), P_{23} micelles with or without EGa1 appear to be superior to the best reported liposomal carrier consisting of PEG_{2000}-DSPE/EPC/EPG (similar $t_{1/2}$ α: 0.5 vs 0.7 h while $t_{1/2}$ β: 18 vs 14 h).[71] This indeed indicates an excellent stability of these micelles in circulation. Most importantly, mTHPC loaded in P_{23} micelles, no matter with or without EGa1, showed a significant increase in half-lives in each corresponding phase, when compared to that of free mTHPC (∼1 vs 0.04 h in the alpha phase and 14 vs 2 h in the beta phase, Table 4). Combined with the significantly enhanced AUC values of micellar mTHPC formulations in each phase (Table 4), this demonstrates the prolonged retention of mTHPC in the circulation resulting from the excellent stability of the P_{23} micelles.

It is worth noting that free mTHPC (i.e., mTHPC dissolved in propylene glycol/PBS 20:30:50 v/v/v) was really difficult for iv injection due to acute mouse responses to relatively high amounts of organic solvent present in a formulation. The administration of free mTHPC clearly led to discomfort in mice, manifested by tachypnea and being passive within 1 min post injection (in fact, two mice died upon iv injection). Such

https://dx.doi.org/10.1021/acs.molpharmaceut.9b01280
Mol. Pharmaceutics 2020, 17, 1276–1292

side effects were also observed in cats with spontaneous squamous cell carcinoma treated with Foscan.[73] In addition, the mice treated with free mTHPC showed the loss of body weight (~1 g on average) 24 h post injection. In contrast, micellar mTHPC formulations were well-tolerated, and none of the micellar mTHPC treated mice showed any side effects during or after their administration. This suggests that the micellar formulations at the injected polymer dose (~1 mg) were safe for *in vivo* applications.

4. CONCLUSIONS

In the present study, PCL-PEG based micelles were decorated with the EGFR-targeted nanobody EGa1 to render this formulation specific for EGFR-overexpressing tumor cells. It is shown that EGa1-conjugated micelles are internalized upon specific binding of the nanobody with the EGFR receptor overexpressed on the surfaces of A431 cells, resulting in enhanced cellular uptake and photocytotoxicity on A431 cells, as compared to EGFR low-expressing HeLa cells. The *in vivo* pharmacokinetic study shows prolonged circulation of mTHPC incorporated in P_{23} micelles, compared to free mTHPC. In conclusion, the conjugation of the EGa1 nanobody to the surfaces of these P_{23} micelles has the potential to significantly improve the selectivity and efficacy of PDT to EGFR-overexpressing tumors.

■ ASSOCIATED CONTENT

Supporting Information

The Supporting Information is available free of charge at https://pubs.acs.org/doi/10.1021/acs.molpharmaceut.9b01280.

^{1}H NMR spectra of the PCL_n oligomers and final PCL_n-PEG/PCL_n-PEG-Mal block copolymers (n = 9, 15, and 23); scheme of synthesis and Cy7 labeling of PCL-PDTC-PEG; further characterization of maleimide incorporation; representative GPC graphs of PCL_9-OH and PCL_9-PEG; details on characterization of Cy7 labeled polymer; LC-ESI-TOF-MS spectra of native and SATA-modified nanobody; SDS-PAGE silver staining of SATA-EGa1 and micelles; EGFR expression on A431 and HeLa cells; confocal images from cells incubated with free mTHPC; cytotoxicity of empty micelles; loading efficiency and loading capacity of targeted and untargeted micelles; EC_{50} of free mTHPC and mTHPC loaded in micelles; evaluation of singlet oxygen generation; fluorescence of mTHPC incorporated in micelles; semilogarithmic plots for pharmacokinetic analysis (PDF)

■ AUTHOR INFORMATION

Corresponding Author

Sabrina Oliveira − *Department of Pharmaceutics, Utrecht Institute for Pharmaceutical Sciences and Division of Cell Biology, Department of Biology, Utrecht University, 3584 CS Utrecht, The Netherlands;* orcid.org/0000-0002-6011-2122; Phone: +31 63 410 3460; Email: S.Oliveira@uu.nl; Fax: +31 30 251 7839

Authors

Yanna Liu − *Department of Pharmaceutics, Utrecht Institute for Pharmaceutical Sciences, Utrecht University, 3584 CS Utrecht, The Netherlands*

Luca Scrivano − *Department of Pharmaceutics, Utrecht Institute for Pharmaceutical Sciences, Utrecht University, 3584 CS Utrecht, The Netherlands*

Julia Denise Peterson − *Department of Pharmaceutics, Utrecht Institute for Pharmaceutical Sciences, Utrecht University, 3584 CS Utrecht, The Netherlands*

Marcel H. A. M. Fens − *Department of Pharmaceutics, Utrecht Institute for Pharmaceutical Sciences, Utrecht University, 3584 CS Utrecht, The Netherlands*

Irati Beltrán Hernández − *Department of Pharmaceutics, Utrecht Institute for Pharmaceutical Sciences and Division of Cell Biology, Department of Biology, Utrecht University, 3584 CS Utrecht, The Netherlands*

Bárbara Mesquita − *Department of Pharmaceutics, Utrecht Institute for Pharmaceutical Sciences, Utrecht University, 3584 CS Utrecht, The Netherlands*

Javier Sastre Toraño − *Department of Chemical Biology & Drug Discovery, Utrecht Institute for Pharmaceutical Sciences, Utrecht University, 3584 CS Utrecht, The Netherlands*

Wim E. Hennink − *Department of Pharmaceutics, Utrecht Institute for Pharmaceutical Sciences, Utrecht University, 3584 CS Utrecht, The Netherlands;* orcid.org/0000-0002-5750-714X

Cornelus F. van Nostrum − *Department of Pharmaceutics, Utrecht Institute for Pharmaceutical Sciences, Utrecht University, 3584 CS Utrecht, The Netherlands;* orcid.org/0000-0003-4210-5241

Complete contact information is available at: https://pubs.acs.org/10.1021/acs.molpharmaceut.9b01280

Notes

The authors declare no competing financial interest.

■ ACKNOWLEDGMENTS

Y.L. is supported by a PhD scholarship from China Scholarship Council (CSC). The authors thank Dr. H. S. de Bruijn and Dr. D. J. Robinson for their assistance with determination of singlet oxygen generation.

■ REFERENCES

(1) Biel, M. A. Photodynamic therapy of head and neck cancer-what's old and what's new. *Handbook of photodynamic therapy: updates on recent applications of porphyrin-based compounds* **2016**, 439−458.

(2) Bray, F.; Ferlay, J.; Soerjomataram, I.; Siegel, R. L.; Torre, L. A.; Jemal, A. Global cancer statistics 2018: GLOBOCAN estimates of incidence and mortality worldwide for 36 cancers in 185 countries. *Ca-Cancer J. Clin.* **2018**, *68* (6), 394−424.

(3) Dirix, P.; Nuyts, S. Evidence-based organ-sparing radiotherapy in head and neck cancer. *Lancet Oncol.* **2010**, *11* (1), 85−91.

(4) Fung, C.; Grandis, J. R. Emerging drugs to treat squamous cell carcinomas of the head and neck. *Expert Opin. Emerging Drugs* **2010**, *15* (3), 355−373.

(5) Marur, S.; Forastiere, A. A. Head and neck squamous cell carcinoma: update on epidemiology, diagnosis, and treatment. *Mayo Clin. Proc.* **2016**, *91* (3), 386−396.

(6) Meulemans, J.; Delaere, P.; Vander Poorten, V. Photodynamic therapy in head and neck cancer: Indications, outcomes, and future prospects. *Curr. Opin Otolaryngol Head Neck Surg* **2019**, *27* (2), 136−141.

(7) Dos Santos, A. F.; De Almeida, D. R. Q.; Terra, L. F.; Baptista, M. S.; Labriola, L. Photodynamic therapy in cancer treatment - an update review. *Journal of Cancer Metastasis and Treatment* **2019**, *5*, 25.

(8) Kwiatkowski, S.; Knap, B.; Przystupski, D.; Saczko, J.; Kedzierska, E.; Knap-Czop, K.; Kotlinska, J.; Michel, O.; Kotowski,

K.; Kulbacka, J. Photodynamic therapy - mechanisms, photosensitizers and combinations. *Biomed. Pharmacother.* **2018**, *106*, 1098−1107.
(9) van Driel, P.; Boonstra, M. C.; Slooter, M. D.; Heukers, R.; Stammes, M. A.; Snoeks, T. J. A.; de Bruijn, H. S.; van Diest, P. J.; Vahrmeijer, A. L.; van Bergen En Henegouwen, P. M. P.; van de Velde, C. J. H.; Lowik, C.; Robinson, D. J.; Oliveira, S. EGFR targeted nanobody-photosensitizer conjugates for photodynamic therapy in a pre-clinical model of head and neck cancer. *J. Controlled Release* **2016**, *229*, 93−105.
(10) Baskaran, R.; Lee, J.; Yang, S. G. Clinical development of photodynamic agents and therapeutic applications. *Biomater Res.* **2018**, *22*, 25.
(11) Hopper, C. Photodynamic therapy: a clinical reality in the treatment of cancer. *Lancet Oncol.* **2000**, *1* (4), 212−219.
(12) de Visscher, S. A.; Kascakova, S.; de Bruijn, H. S.; van den Heuvel, A.; Amelink, A.; Sterenborg, H. J.; Robinson, D. J.; Roodenburg, J. L.; Witjes, M. J. Fluorescence localization and kinetics of mTHPC and liposomal formulations of mTHPC in the window-chamber tumor model. *Lasers Surg. Med.* **2011**, *43* (6), 528−536.
(13) Bovis, M. J.; Woodhams, J. H.; Loizidou, M.; Scheglmann, D.; Bown, S. G.; Macrobert, A. J. Improved *in vivo* delivery of m-THPC via pegylated liposomes for use in photodynamic therapy. *J. Controlled Release* **2012**, *157* (2), 196−205.
(14) Redmond, R. W.; Land, E. J.; Truscott, T. G. Aggregation effects on the photophysical properties of porphyrins in relation to mechanisms involved in photodynamic therapy. *Advances in experimental medicine and biology* **1985**, *193*, 293−302.
(15) Triesscheijn, M.; Ruevekamp, M.; Out, R.; Van Berkel, T. J.; Schellens, J.; Baas, P.; Stewart, F. A. The pharmacokinetic behavior of the photosensitizer meso-tetra-hydroxyphenyl-chlorin in mice and men. *Cancer Chemother. Pharmacol.* **2007**, *60* (1), 113−122.
(16) Dos Santos, N.; Allen, C.; Doppen, A. M.; Anantha, M.; Cox, K. A.; Gallagher, R. C.; Karlsson, G.; Edwards, K.; Kenner, G.; Samuels, L.; Webb, M. S.; Bally, M. B. Influence of poly(ethylene glycol) grafting density and polymer length on liposomes: relating plasma circulation lifetimes to protein binding. *Biochim. Biophys. Acta, Biomembr.* **2007**, *1768* (6), 1367−1377.
(17) Klibanov, A. L.; Maruyama, K.; Torchilin, V. P.; Huang, L. Amphipathic polyethyleneglycols effectively prolong the circulation time of liposomes. *FEBS Lett.* **1990**, *268* (1), 235−237.
(18) Torchilin, V. P. Recent advances with liposomes as pharmaceutical carriers. *Nat. Rev. Drug Discovery* **2005**, *4* (2), 145−160.
(19) Maeda, H.; Wu, J.; Sawa, T.; Matsumura, Y.; Hori, K. Tumor vascular permeability and the EPR effect in macromolecular therapeutics: a review. *J. Controlled Release* **2000**, *65* (1), 271−284.
(20) Fang, J.; Nakamura, H.; Maeda, H. The EPR effect: Unique features of tumor blood vessels for drug delivery, factors involved, and limitations and augmentation of the effect. *Adv. Drug Delivery Rev.* **2011**, *63* (3), 136−151.
(21) Maeda, H. Toward a full understanding of the EPR effect in primary and metastatic tumors as well as issues related to its heterogeneity. *Adv. Drug Delivery Rev.* **2015**, *91*, 3−6.
(22) Reshetov, V.; Lassalle, H. P.; Francois, A.; Dumas, D.; Hupont, S.; Grafe, S.; Filipe, V.; Jiskoot, W.; Guillemin, F.; Zorin, V.; Bezdetnaya, L. Photodynamic therapy with conventional and PEGylated liposomal formulations of mTHPC (temoporfin): Comparison of treatment efficacy and distribution characteristics in vivo. *Int. J. Nanomed.* **2013**, *8*, 3817−3831.
(23) Cabral, H.; Matsumoto, Y.; Mizuno, K.; Chen, Q.; Murakami, M.; Kimura, M.; Terada, Y.; Kano, M. R.; Miyazono, K.; Uesaka, M.; Nishiyama, N.; Kataoka, K. Accumulation of sub-100 nm polymeric micelles in poorly permeable tumours depends on size. *Nat. Nanotechnol.* **2011**, *6* (12), 815−823.
(24) Danhier, F. To exploit the tumor microenvironment: Since the EPR effect fails in the clinic, what is the future of nanomedicine? *J. Controlled Release* **2016**, *244* (Pt A), 108−121.
(25) Jain, R. K.; Stylianopoulos, T. Delivering nanomedicine to solid tumors. *Nat. Rev. Clin. Oncol.* **2010**, *7* (11), 653−664.
(26) Jiang, W.; Kim, B. Y.; Rutka, J. T.; Chan, W. C. Nanoparticle-mediated cellular response is size-dependent. *Nat. Nanotechnol.* **2008**, *3* (3), 145−150.
(27) Yuan, F.; Leunig, M.; Huang, S. K.; Berk, D. A.; Papahadjopoulos, D.; Jain, R. K. Microvascular permeability and interstitial penetration of sterically stabilized (stealth) liposomes in a human tumor xenograft. *Cancer Res.* **1994**, *54* (13), 3352−3356.
(28) Deng, C.; Jiang, Y.; Cheng, R.; Meng, F.; Zhong, Z. Biodegradable polymeric micelles for targeted and controlled anticancer drug delivery: Promises, progress and prospects. *Nano Today* **2012**, *7* (5), 467−480.
(29) Varela-Moreira, A.; Shi, Y.; Fens, M. H. A. M.; Lammers, T.; Hennink, W. E.; Schiffelers, R. M. Clinical application of polymeric micelles for the treatment of cancer. *Materials Chemistry Frontiers* **2017**, *1* (8), 1485−1501.
(30) Cabral, H.; Kataoka, K. Progress of drug-loaded polymeric micelles into clinical studies. *J. Controlled Release* **2014**, *190*, 465−476.
(31) Houdaihed, L.; Evans, J. C.; Allen, C. Overcoming the road blocks: advancement of block copolymer micelles for cancer therapy in the clinic. *Mol. Pharmaceutics* **2017**, *14* (8), 2503−2517.
(32) Gaucher, G.; Dufresne, M. H.; Sant, V. P.; Kang, N.; Maysinger, D.; Leroux, J. C. Block copolymer micelles: Preparation, characterization and application in drug delivery. *J. Controlled Release* **2005**, *109* (1−3), 169−188.
(33) Park, J. H.; Lee, S.; Kim, J.-H.; Park, K.; Kim, K.; Kwon, I. C. Polymeric nanomedicine for cancer therapy. *Prog. Polym. Sci.* **2008**, *33* (1), 113−137.
(34) Bagheri, M.; Bresseleers, J.; Varela-Moreira, A.; Sandre, O.; Meeuwissen, S. A.; Schiffelers, R. M.; Metselaar, J. M.; van Nostrum, C. F.; van Hest, J. C. M.; Hennink, W. E. Effect of formulation and processing parameters on the size of mPEG- b-p(HPMA-Bz) polymeric micelles. *Langmuir* **2018**, *34* (50), 15495−15506.
(35) Danhier, F.; Feron, O.; Preat, V. To exploit the tumor microenvironment: Passive and active tumor targeting of nanocarriers for anti-cancer drug delivery. *J. Controlled Release* **2010**, *148* (2), 135−146.
(36) Chang, E.; Yu, W. W.; Colvin, V. L.; Drezek, R. Quantifying the influence of surface coatings on quantum dot uptake in cells. *J. Biomed. Nanotechnol.* **2005**, *1* (4), 397−401.
(37) Pirollo, K. F.; Chang, E. H. Does a targeting ligand influence nanoparticle tumor localization or uptake? *Trends Biotechnol.* **2008**, *26* (10), 552−558.
(38) Talelli, M.; Rijcken, C. J.; Oliveira, S.; van der Meel, R.; van Bergen En Henegouwen, P. M.; Lammers, T.; van Nostrum, C. F.; Storm, G.; Hennink, W. E. Nanobody-shell functionalized thermosensitive core-crosslinked polymeric micelles for active drug targeting. *J. Controlled Release* **2011**, *151* (2), 183−192.
(39) Martinez-Jothar, L.; Beztsinna, N.; van Nostrum, C. F.; Hennink, W. E.; Oliveira, S. Selective cytotoxicity to HER2 positive breast cancer cells by saporin-loaded nanobody-targeted polymeric nanoparticles in combination with photochemical internalization. *Mol. Pharmaceutics* **2019**, *16* (4), 1633−1647.
(40) Ruoslahti, E.; Bhatia, S. N.; Sailor, M. J. Targeting of drugs and nanoparticles to tumors. *J. Cell Biol.* **2010**, *188* (6), 759−768.
(41) Zimmermann, M.; Zouhair, A.; Azria, D.; Ozsahin, M. The epidermal growth factor receptor (EGFR) in head and neck cancer: its role and treatment implications. *Radiat. Oncol.* **2006**, *1*, 11.
(42) Dolk, E.; van Vliet, C.; Perez, J. M.; Vriend, G.; Darbon, H.; Ferrat, G.; Cambillau, C.; Frenken, L. G.; Verrips, T. Induced refolding of a temperature denatured llama heavy-chain antibody fragment by its antigen. *Proteins: Struct., Funct., Genet.* **2005**, *59* (3), 555−564.
(43) Oliveira, S.; Schiffelers, R. M.; van der Veeken, J.; van der Meel, R.; Vongpromek, R.; van Bergen En Henegouwen, P. M.; Storm, G.; Roovers, R. C. Downregulation of EGFR by a novel multivalent nanobody-liposome platform. *J. Controlled Release* **2010**, *145* (2), 165−175.

https://dx.doi.org/10.1021/acs.molpharmaceut.9b01280
Mol. Pharmaceutics 2020, 17, 1276−1292

(44) Oliveira, S.; Heukers, R.; Sornkom, J.; Kok, R. J.; van Bergen en Henegouwen, P. M. P. Targeting tumors with nanobodies for cancer imaging and therapy. *J. Controlled Release* **2013**, *172* (3), 607−617.
(45) Gao, H.; Shi, W.; Freund, L. B. Mechanics of receptor-mediated endocytosis. *Proc. Natl. Acad. Sci. U. S. A.* **2005**, *102* (27), 9469−9474.
(46) Prabha, S.; Zhou, W. Z.; Panyam, J.; Labhasetwar, V. Size-dependency of nanoparticle-mediated gene transfection: Studies with fractionated nanoparticles. *Int. J. Pharm.* **2002**, *244* (1−2), 105−115.
(47) Zhang, S.; Li, J.; Lykotrafitis, G.; Bao, G.; Suresh, S. Size-dependent endocytosis of nanoparticles. *Adv. Mater.* **2009**, *21*, 419−424.
(48) Sykes, E. A.; Chen, J.; Zheng, G.; Chan, W. C. W. Investigating the impact of nanoparticle size on active and passive tumor targeting efficiency. *ACS Nano* **2014**, *8* (6), 5696−5706.
(49) van Lith, S. A.; van Duijnhoven, S. M.; Navis, A. C.; Leenders, W. P.; Dolk, E.; Wennink, J. W.; van Nostrum, C. F.; van Hest, J. C. Legomedicine-a versatile chemo-enzymatic approach for the preparation of targeted dual-labeled llama antibody-nanoparticle conjugates. *Bioconjugate Chem.* **2017**, *28* (2), 539−548.
(50) Ravasco, J.; Faustino, H.; Trindade, A.; Gois, P. M. P. Bioconjugation with maleimides: A useful tool for chemical biology. *Chem. - Eur. J.* **2019**, *25* (1), 43−59.
(51) Wennink, J. W. H.; Liu, Y.; Makinen, P. I.; Setaro, F.; de la Escosura, A.; Bourajjaj, M.; Lappalainen, J. P.; Holappa, L. P.; van den Dikkenberg, J. B.; Al Fartousi, M.; Trohopoulos, P. N.; Yla-Herttuala, S.; Torres, T.; Hennink, W. E.; van Nostrum, C. F. Macrophage selective photodynamic therapy by meta-tetra(hydroxyphenyl)chlorin loaded polymeric micelles: A possible treatment for cardiovascular diseases. *Eur. J. Pharm. Sci.* **2017**, *107*, 112−125.
(52) Couffin, A.; Delcroix, D.; Martín-Vaca, B.; Bourissou, D.; Navarro, C. Mild and efficient preparation of block and gradient copolymers by methanesulfonic acid catalyzed ring-opening polymerization of caprolactone and trimethylene carbonate. *Macromolecules* **2013**, *46* (11), 4354−4360.
(53) Delcroix, D.; Martin-Vaca, B.; Bourissou, D.; Navarro, C. Ring-opening polymerization of trimethylene carbonate catalyzed by methanesulfonic acid: Activated monomer versus active chain end mechanisms. *Macromolecules* **2010**, *43* (21), 8828−8835.
(54) Hofman, E. G.; Ruonala, M. O.; Bader, A. N.; van den Heuvel, D.; Voortman, J.; Roovers, R. C.; Verkleij, A. J.; Gerritsen, H. C.; van Bergen En Henegouwen, P. M. EGF induces coalescence of different lipid rafts. *J. Cell Sci.* **2008**, *121* (Pt 15), 2519−2528.
(55) van der Meel, R.; Oliveira, S.; Altintas, I.; Haselberg, R.; van der Veeken, J.; Roovers, R. C.; van Bergen en Henegouwen, P. M.; Storm, G.; Hennink, W. E.; Schiffelers, R. M.; Kok, R. J. Tumor-targeted nanobullets: Anti-EGFR nanobody-liposomes loaded with anti-IGF-1R kinase inhibitor for cancer treatment. *J. Controlled Release* **2012**, *159* (2), 281−289.
(56) Yin, H.; Lee, E. S.; Kim, D.; Lee, K. H.; Oh, K. T.; Bae, Y. H. Physicochemical characteristics of pH-sensitive poly(L-histidine)-*b*-poly(ethylene glycol)/poly(L-lactide)-*b*-poly(ethylene glycol) mixed micelles. *J. Controlled Release* **2008**, *126* (2), 130−138.
(57) Ehrhart, J.; Mingotaud, A. F.; Violleau, F. Asymmetrical flow field-flow fractionation with multi-angle light scattering and quasi elastic light scattering for characterization of poly(ethyleneglycol-b-varepsilon-caprolactone) block copolymer self-assemblies used as drug carriers for photodynamic therapy. *J. Chromatogr A* **2011**, *1218* (27), 4249−4256.
(58) Shi, Y.; van Steenbergen, M. J.; Teunissen, E. A.; Novo, L.; Gradmann, S.; Baldus, M.; van Nostrum, C. F.; Hennink, W. E. π-π stacking increases the stability and loading capacity of thermosensitive polymeric micelles for chemotherapeutic drugs. *Biomacromolecules* **2013**, *14* (6), 1826−1837.
(59) Carstens, M. G.; Bevernage, J. J. L.; van Nostrum, C. F.; van Steenbergen, M. J.; Flesch, F. M.; Verrijk, R.; de Leede, L. G. J.; Crommelin, D. J. A.; Hennink, W. E. Small oligomeric micelles based on end group modified mPEG-oligocaprolactone with monodisperse hydrophobic blocks. *Macromolecules* **2007**, *40* (1), 116−122.
(60) Carstens, M. G.; van Nostrum, C. F.; Verrijk, R.; de Leede, L. G.; Crommelin, D. J.; Hennink, W. E. A mechanistic study on the chemical and enzymatic degradation of PEG-Oligo(ε-caprolactone) micelles. *J. Pharm. Sci.* **2008**, *97* (1), 506−518.
(61) Lassalle, H. P.; Wagner, M.; Bezdetnaya, L.; Guillemin, F.; Schneckenburger, H. Fluorescence imaging of Foscan and Foslip in the plasma membrane and in whole cells. *J. Photochem. Photobiol., B* **2008**, *92* (1), 47−53.
(62) Reidy, K.; Campanile, C.; Muff, R.; Born, W.; Fuchs, B. mTHPC-mediated photodynamic therapy is effective in the metastatic human 143B osteosarcoma cells. *Photochem. Photobiol.* **2012**, *88* (3), 721−727.
(63) Chen, Y.; Tezcan, O.; Li, D.; Beztsinna, N.; Lou, B.; Etrych, T.; Ulbrich, K.; Metselaar, J. M.; Lammers, T.; Hennink, W. E. Overcoming multidrug resistance using folate receptor-targeted and pH-responsive polymeric nanogels containing covalently entrapped doxorubicin. *Nanoscale* **2017**, *9* (29), 10404−10419.
(64) Xie, J.; Xu, C.; Kohler, N.; Hou, Y.; Sun, S. Controlled PEGylation of monodisperse Fe_3O_4 nanoparticles for reduced non-specific uptake by macrophage cells. *Adv. Mater.* **2007**, *19* (20), 3163−3166.
(65) Kiesslich, T.; Berlanda, J.; Plaetzer, K.; Krammer, B.; Berr, F. Comparative characterization of the efficiency and cellular pharmacokinetics of Foscan- and Foslip-based photodynamic treatment in human biliary tract cancer cell lines. *Photochem. Photobiol. Sci.* **2007**, *6* (6), 619−627.
(66) Syu, W. J.; Yu, H. P.; Hsu, C. Y.; Rajan, Y. C.; Hsu, Y. H.; Chang, Y. C.; Hsieh, W. Y.; Wang, C. H.; Lai, P. S. Improved photodynamic cancer treatment by folate-conjugated polymeric micelles in a KB xenografted animal model. *Small* **2012**, *8* (13), 2060−2069.
(67) Moret, F.; Scheglmann, D.; Reddi, E. Folate-targeted PEGylated liposomes improve the selectivity of PDT with meta-tetra(hydroxyphenyl)chlorin (m-THPC). *Photochemical & photobiological sciences: Official journal of the European Photochemistry Association and the European Society for Photobiology* **2013**, *12* (5), 823−834.
(68) Wu, J.; Feng, S.; Liu, W.; Gao, F.; Chen, Y. Targeting integrin-rich tumors with temoporfin-loaded vitamin-E-succinate-grafted chitosan oligosaccharide/d-alpha-tocopheryl polyethylene glycol 1000 succinate nanoparticles to enhance photodynamic therapy efficiency. *Int. J. Pharm.* **2017**, *528* (1−2), 287−298.
(69) Paszko, E.; Vaz, G. M.; Ehrhardt, C.; Senge, M. O. Transferrin conjugation does not increase the efficiency of liposomal Foscan during in vitro photodynamic therapy of oesophageal cancer. *Eur. J. Pharm. Sci.* **2013**, *48* (1−2), 202−210.
(70) Cramers, P.; Ruevekamp, M.; Oppelaar, H.; Dalesio, O.; Baas, P.; Stewart, F. A. Foscan uptake and tissue distribution in relation to photodynamic efficacy. *Br. J. Cancer* **2003**, *88* (2), 283−290.
(71) Decker, C.; Schubert, H.; May, S.; Fahr, A. Pharmacokinetics of temoporfin-loaded liposome formulations: correlation of liposome and temoporfin blood concentration. *J. Controlled Release* **2013**, *166* (3), 277−285.
(72) Shi, Y.; van der Meel, R.; Theek, B.; Oude Blenke, E.; Pieters, E. H.; Fens, M. H.; Ehling, J.; Schiffelers, R. M.; Storm, G.; van Nostrum, C. F.; Lammers, T.; Hennink, W. E. Complete regression of xenograft tumors upon targeted delivery of paclitaxel via Pi-Pi stacking stabilized polymeric micelles. *ACS Nano* **2015**, *9* (4), 3740−3752.
(73) Buchholz, J.; Kaser-Hotz, B.; Khan, T.; Rohrer Bley, C.; Melzer, K.; Schwendener, R. A.; Roos, M.; Walt, H. Optimizing photodynamic therapy: in vivo pharmacokinetics of liposomal meta-(tetrahydroxyphenyl)chlorin in feline squamous cell carcinoma. *Clin. Cancer Res.* **2005**, *11* (20), 7538−7544.

https://dx.doi.org/10.1021/acs.molpharmaceut.9b01280
Mol. Pharmaceutics 2020, 17, 1276−1292